Applied Catalysis B: Environment and Energy 349 (2024) 123865

Contents lists available at ScienceDirect

Applied Catalysis B: Environment and Energy

journal homepage: www.elsevier.com/locate/apcatb

Ethanol to gasoline and sustainable aviation fuel precursors: an innovative cascade strategy over Zr-based multifunctional catalysts in the gas phase

Anna Gagliardi [a,b], Giulia Balestra [a,b], Jacopo De Maron [a,b], Rita Mazzoni [a,b,c], Tommaso Tabanelli [a,b,c,*], Fabrizio Cavani [a,b,c]

[a] Dipartimento di Chimica Industriale "Toso Montanari", viale Risorgimento, 4, Bologna 40136, Italy
[b] Center for Chemical Catalysis-C3, University of Bologna, viale del Risorgimento 4, Bologna, 40136, Italy
[c] Interdepartmental Centre for Industrial Research, Renewable Sources Environment, Sea, Energy (CIRI-FRAME), viale Risorgimento, 4, Bologna 40136, Italy

ARTICLE INFO

Keywords:
Ethanol upgrading
Heterogeneous catalysis
Copper on zirconia catalyst
Continuous-flow
Sustainable aviation fuels

ABSTRACT

In the biorefinery context, bioethanol upgrading has been identified as a valuable approach to develop a circular economy for fuels and chemicals production. In this work, the gas-phase, continuous flow catalytic upgrading of ethanol to blends with features close to those suitable for jet fuel is tackled through an innovative strategy based on the promotion of several reactions in cascade. Catalytic transfer hydrogenation, aldol condensation, dehydrogenative coupling, and ketonization reactions were combined in a one-pot approach over a relatively simple and cheap catalytic system consisting of copper nanoparticles supported on zirconium (and lanthanum) oxides. The resulting cascade reaction scheme led to the production of a blend of oxygenated adducts in the C6-C14 range with promising properties for use as jet fuel. By tailoring the features of the non-innocent support and/or co-feeding hydrogen to the reactor, up to 40% selectivity for the jet fuel range fraction, with ethanol conversion above 85%, was achieved during the first 6 h of time on stream, simultaneously enhancing catalyst stability and lifetime.

1. Introduction

The production of alternative fuels from biomass is a topic of enormous interest for both academic and industrial research, due to the urgency to break free from fossil resources and achieve a more sustainable circular economy.

Two types of fuel are used in combustion engines: ignition fuels and compression fuels. Ignition fuels are a mixture of lighter, more volatile compounds that require a specific ignition source to burn controllably and include aviation (AvGas) and automotive (MoGas) gasolines [1]. Compression fuels, on the other hand, contain a wider variety of carbon chains that are more stable under a wider range of temperatures and pressures [2]. Diesel, Kerosene, and Jet fuel (which is a tightly standardized, high-quality variant of kerosene) are examples of such fuels. While automotive only relies on piston engines, which can burn compression or ignition fuels depending on their design, aircrafts can apply piston or turbine engines. Piston engines are mostly found in small aircraft, whereas large modern aircraft generally use turbines. Since turbines can only burn compression fuel, they all run on jet fuel. A more detailed description of the different types and properties of jet fuels is reported in a dedicated chapter in the Electronic Supporting Information (ESI).

Even though the distillation of crude oil remains the prevalent manufacturing pathway for jet fuel production, innovative processes to obtain Sustainable Aviation Fuels (SAFs) starting from alternative, renewable sources are currently under investigation worldwide and, in few cases, have already found their slice of the market. This is also due to the ambitious targets set both by the US and the European Union aimed to tackle climate change. In this context, the EU Green Deal led the way for making the EU's energy, transport and land use policies fit for reducing net greenhouse gas emissions by at least 55% by 2030, compared with 1990 levels. This proposal includes a plan to achieve a more sustainable air transport, known as the "ReFuelEU" Aviation initiative [3].

For instance, SAFs production may derive from processes known for a century: Fischer-Tropsch (FT) can indeed be used to produce liquid hydrocarbon fuels from syngas obtained by biomass gasification, and good selectivity for jet fuel fraction is obtained at low temperature

* Corresponding author at: Dipartimento di Chimica Industriale "Toso Montanari", viale Risorgimento, 4, Bologna 40136, Italy.
E-mail address: tommaso.tabanelli@unibo.it (T. Tabanelli).

https://doi.org/10.1016/j.apcatb.2024.123865
Received 14 November 2023; Received in revised form 12 February 2024; Accepted 19 February 2024
Available online 20 February 2024

(210–260 °C). FT aviation fuel might decrease emissions [4], but the low aromatic content and less energy density can cause leakage problems and low efficiency. On the other hand, lignocellulosic materials have been studied as raw materials due to their worldwide availability. A few examples of hydroprocessed depolymerized cellulosic jet (HDCJ) or fuels obtained from the hydrodeoxygenation and hydrogenation treatments on lignin-derived bio-oil are reported elsewhere [5,6], even though these technologies still present drawbacks such as high hydrogen consumption and low yields. Other possible SAFs production pathways include hydrothermal liquefaction (HTL) or catalytic hydrothermolysis (CH) of algal or oil plant and direct sugar to hydrocarbons (DSHC) processes [7]. The manufacture of fuels starting from vegetable oils or animal fats (hydrogenated esters and fatty acids, HEFA) has been broadly investigated in the literature and applied industrially [8], but an extensive use of such resources for jet fuel manufacture would lead to an increased cost of these raw materials with negative consequences for all the oleochemicals companies involved in the production of value added chemicals (e.g., bio-polymers, lubricants and cosmetics). Recently, a study [9] described the production of SAF via a multistep process involving i) arrested methanogenesis of wet waste to obtain C_3-C_8 volatile fatty acids (VFAs), ii) ketonization of VFAs to C_8-C_{15} linear ketones, iii) aldol condensation of linear ketones towards branched and cyclic enones, iv) HDO of the fractions obtained after step ii) and step iii). Unfortunately, the economic viability of this approach is hindered by the expensive purification of VFA, which are too diluted in fermented waste streams in low concentrations (e.g., 1 wt%) to be directly processed; moreover, fermented streams contain significant amounts of inorganic salts that might poison a solid catalyst [10].

For all these reasons, the production of blends that can be used as jet fuel starting from bioethanol (bioEtOH) constitutes a new and highly promising alternative. Nowadays, bioEtOH is produced mainly from agricultural crops such as corn, sugarcane, and sugar-beet which require large cultivation areas [11,12]. Since the above crops are also used for human food supply, such first generation ethanol production can decrease food availability while increasing the prices. The increasing awareness of this problem drove the research interest towards the production of second generation bioEtOH, which can be produced from the inedible parts of plants (i.e., cellulose) [13] or food industry wastes [14], or even third generation EtOH from marine organisms such as algae [15,16].

Proof of the massive interest in the EtOH to SAFs conversion is given by very recent patents and publications dealing with the subject. The main synthetic strategies patented to date, together with that reported herein, are summarized in both Scheme 1 and Table S3. In a series of patents by Vertimass, issued between 2016 and 2021, C. E. Wyman *et al.* tackled the condensation and dehydration of alcohols to aromatic compounds and a mixture of hydrocarbons (from C5 upwards) for fuel application, following the "hydrocarbon pool" pathway [17,18] over zeolites modified with a variety of cations including alkali and alkaline earth metals, transition metals and lanthanides. The main examples reported featured V-ZSM-5 and Ga-ZSM-5 catalysts (Scheme 1**a**). They also patented systems and methods to reduce energy and water consumption through heat transfer and recovery [19–22]. In 2017, a patent issued to Battelle Memorial Institute, operating agency of the Pacific Northwest National Laboratory (PNNL), disclosed a new process for the selective conversion of ethanol (or ethylene) containing feedstocks to fuel-range hydrocarbons (including jet fuels), via either one-pot or two stage dehydration and oligomerization processes. While dehydrations are catalyzed by acid catalysts (i.e. acid zeolites), oligomerization are promoted by supported Ni catalysts over a range of acid aluminosilicates and silicas and lead to the formation of C4-C23 blends which are finally hydrogenated (e.g. over Pt/Al_2O_3) to obtain the saturated fuels (Scheme 1**b**) [23]. As an alternative, in 2020 also $Ag\text{-}ZrO_2/SiO_2$ catalytic system was found to be able to convert EtOH into a butenes-rich mixture that can be lately oligomerized to longer hydrocarbons for jet fuel application [24]. The so obtained blend fueled a Virgin Atlantic commercial

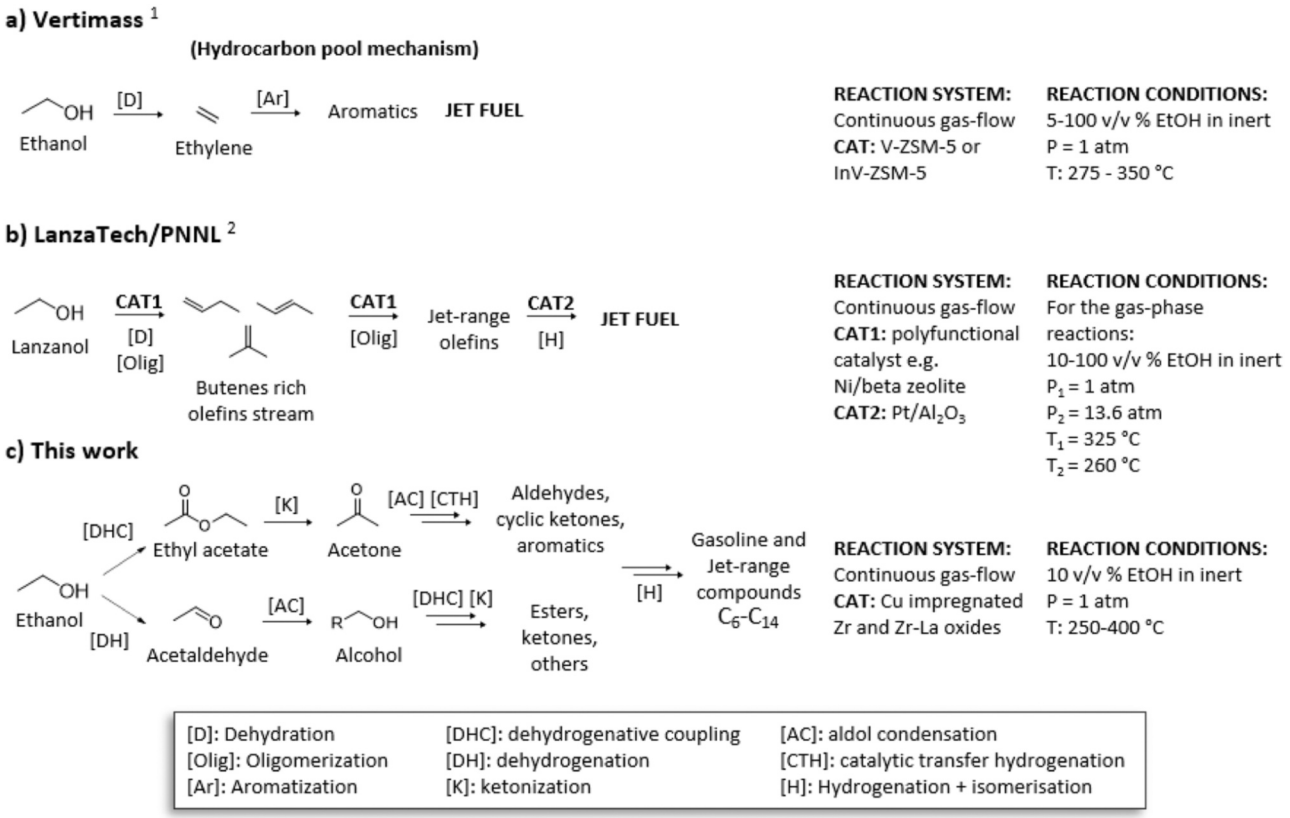

Scheme 1. Different synthetic approach for the production of SAFs from ethanol. [1]References [25–28]. [2]References [23,29–32].

passenger flight from Orlando to London in late 2018 and, in late 2019, a new plane purchased by All Nippon Airways, which flew from Seattle to Tokyo.

Noticeably, the aforementioned literature is focused on the production of conventional, kerosene-based jet fuel blends. Unlike road transport, the implications of utilizing alternative jet fuels which carry a high percentage of oxygenated compounds remains to date scarcely explored, due to the complexity and large investments involved in research on real aeronautical turbines.

Some studies demonstrated that blending conventional jet fuel with oxygenated compounds can be unharmful to the engine or even beneficial to a certain extent. In particular, Habib et al. [33] fed a selection of pure methyl esters (soy methyl ester, canola methyl ester and recycled rapeseed methyl ester) and their blends with Jet A fuel (50% biofuel by volume) to an unmodified small-scale gas turbine, in order to understand the impact on performance and emissions of the engine. The results showed that static thrust of pure esters and blends with Jet A was comparable to that of pure Jet A. At the same time, CO and NO pollutant emission concentrations decreased when bioesters were added to Jet A and pure bioesters showed higher thermal efficiencies than Jet A and the blends. Therefore, even though so far some of the properties such as thermal stability and freezing point of oxygenated fuels have proven inferior compared to conventional fuel, more investigation is certainly worth in this field.

In a patent from 2019, PNNL researchers claimed a method for upgrading an EtOH containing feedstock to a mixture of higher ketones and alcohols over Pd-promoted ZnO-ZrO_2 and CuO-MgO-Al_2O_3 [34]. These products are considered key intermediates for the synthesis of both innovative lubricants and alternative fuels from renewables. In particular, the inventors acknowledged ketones as suitable building blocks for producing infrastructure compatible hydrocarbon fuels (including jet fuel), but also pointed out their high energy density, that could promote them as a standalone alternative to hydrocarbons. In a follow up publication [35], the same authors reported on the selective synthesis of aliphatic ketones, in particular linear, with chain lengths between C5 and C11 starting from ethanol. More details were disclosed about the catalytic system, consisting of Pd (even only 0.1 wt%) supported on a solid mixture of ZnO and ZrO_2. In 2020, Battelle Memorial Institute and K. Kallupalayam et al. also patented a process for ethanol upgrading to mixtures of higher alcohols over copper, magnesium and aluminum oxide-based catalysts (CuO-MgO-Al_2O_3), with operative conditions including 13–14 bar of hydrogen pressure, which enhances the selectivity for higher alcohols, and temperatures between 275 and 350 °C [36]. Finally, the same authors disclosed in a recent patent [37] a process involving the production of SAF in three-step via ethanol condensation over Pd-promoted ZnO-ZrO_2, dimerization/trimerization of the resulting ketones over Pd-promoted MgO-Al_2O_3 and a final hydrodeoxygenation over Ni-based catalyst exploiting the H_2 co-produced during the previous steps (for instance, by the dehydrogenation of EtOH to acetaldehyde).

The production of SAF starting from biobased EtOH as feedstock is attractive in respect to the other pathway cited previously it is based on a well-established technology, while biomass gasification, hydrothermal liquefaction of lignocellulose/algae, hydrodeoxygenation of bio-oils and arrested methanogenesis of wet waste to VFAs does not have the same industrial maturity. On the other hand, EtOH is obtained as a pure product or an aqueous solution, while the other methods usually produce mixture of compounds, making the upgrading process more complex. Finally, to meet international specifications on jet fuels properties SAF must contain both linear and branched hydrocarbon as well as aromatics, which can all be obtained by means of EtOH condensation/hydrodeoxygenation [37] in satisfactory proportions, while this is not the case, for instance, of liquid hydrocarbons produced via FT of syngas obtained by gasification.

ZrO_2, which is featured in previously cited patent and paper from PNNL researchers, is considered a safe material and it is widely used in catalysis. Furthermore, ZrO_2 production has a low impact compared to other commonly used catalysts. In fact, its supply chain require few production steps and the mining and beneficiation processes for Zirconium are minimally intensive due to the very high initial Zirconium content (10–20%) in heavy-mineral sands [38].

The functionalization of ZrO_2 with copper, which is cheaper than noble metals and is also considered as a low toxicity element with respect to, for example, Ni, leads to versatile copper-zirconia systems which have been studied as catalysts for several reactions, including CO_2 and CO valorization through methanol synthesis [39–41], methanol [42,43] and ethanol [44,45] steam reforming, methanol decomposition for hydrogen production [46,47], catalytic combustion of toluene [48] and the emerging (bio)alcohol upgrading route via dehydrogenative coupling (DHC) reaction [49,50]. The latter transformation, which has been attracting increasing attention, consists of the direct conversion of two molecules of alcohol into the corresponding symmetrical ester, along with the production of two molecules of H_2 (Scheme 2).

In recent years, transformation of carboxylic acids and/or esters to ketones by means of ketonization (Scheme 3) has been investigated as an effective tool for reducing oxygen content in biobased molecules without consuming valuable hydrogen [51]. Alongside, the discovery that several classes of endophytic fungi can convert cellulosic biomass to a range of other oxygenated molecules, which are potentially viable as biofuels, gave rise to various studies above the combustion properties of ketones [52,53].

Since our group recently found that ZrO_2 can be effectively applied both for the continuous-flow, gas-phase ketonization of propionic acid to 3-pentanone [54], and for the catalytic transfer hydrogenation (CTH) of alkyl levulinates with ethanol [55–57], we glimpsed the possibility to further improve this material by the impregnation of a redox active metal such as copper, this way promoting a complex cascade series of reactions over the same catalyst. This “one-pot” strategy is not aimed to selectively produce a single molecule but rather leads to the direct production of a mixture of compounds valuable for SAFs application. In particular, the reactions involved include: i) alcohol dehydrogenation to aldehyde, ii) alcohol direct coupling to esters through DHC, feasible over Cu supported catalysts as demonstrated by the work of Scotti et al. [49], iii) ketonization, which can transform those esters into ketones [58], iv) consecutive aldol condensation of esters/ketones with acetaldehyde and other longer aldehydes and v) CTH reactions, paving the way for EtOH upgrading to a blend of linear and branched longer chain compounds with a carbon number and properties suitable for jet fuel application.

For all these reasons, herein we report for the first time in literature about the continuous-flow, gas-phase ethanol upgrading at atmospheric pressure over a relatively cheap and simple metallic Cu supported over Zr (and/or La) based oxides. Being these materials multifunctional (i.e., redox, acid and base) catalytic systems, they are able to promote the aforementioned cascade series of reactions in relatively mild conditions (Scheme 1**c**). The final products mixtures, containing linear and branched esters, linear and branched alcohols, linear, branched and cyclic ketones, aldehydes, alkenes and aromatics (hydrocarbons and phenolics), showed similar properties in terms of density, gross heat of combustion, flash point, freezing point and aromatics content, to those of Jet A and A-1 fuels, which are the most widespread worldwide. Even though more work is needed to optimize the catalytic material, increasing its lifetime and fostering acetaldehyde conversion, the obtained blends could be potentially used as jet fuel or jet fuel additive after a few preliminary operations such as the distillation of the lighter compounds and a mild hydrogenation process in order to stabilize aldehydes and unsaturated compounds.

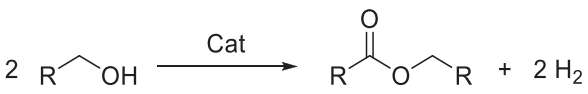

Scheme 2. General scheme of the DHC reaction.

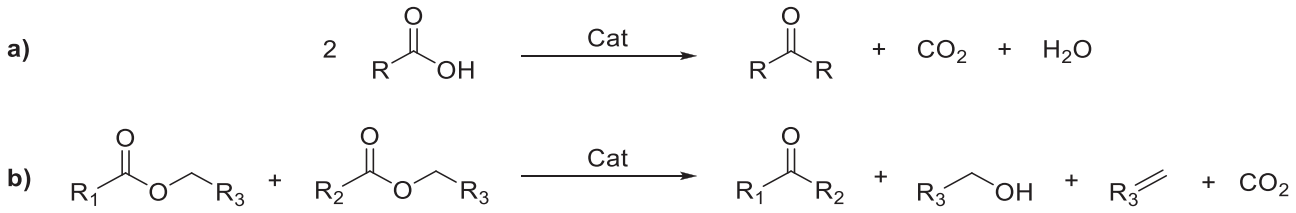

Scheme 3. General scheme of a) carboxylic acid and b) ester ketonization.

2. Experimental section

Please see ESI for any detail related to the materials and reagents used in this work as well as for further details on catalysts preparation and characterization.

2.1. Catalyst preparation

t-ZrO_2 and *m*-ZrO_2 were prepared by precipitation in alkaline environment [56,57] and hydrothermal synthesis [59], respectively, according to previously reported procedures.

La-Zr-O was synthesized by co-precipitation at pH 10–12. Targeting a La:Zr atomic ratio of 0.19, a 0.3 M solution (206 mL) of $La(NO_3)_3{\cdot}6H_2O$ and $ZrO(NO_3)_2{\cdot}2H_2O$ was added dropwise to a 5 M solution (185 mL) of NH_3. The precipitate was digested for 72 h at 100 °C, by keeping the pH value at 11.5 with a continuous addition of concentrated (28% wt) NH_3 aqueous solution with a syringe pump (KDScientific Legacy Syringe-infusion Pump). The sample was then filtered, washed thoroughly with NH_3 3 M, oven dried at 100 °C, and calcined at 450 °C for 12 h with a 5 °C/min heating ramp.

For the synthesis of La_2O_3, $La(NO_3)_3{\cdot}6H_2O$ was dissolved in deionized water to obtain a 0.5 mol/L solution (60 mL); such solution was slowly added dropwise to aqueous NH_3 (2 mol/L, 300 mL) under vigorous stirring. The pH of the basic solution was maintained constant and equal to 11.5 during the addition by adding concentrated NH_3 (28–30 wt%). Precipitates were aged for 1–2 h under stirring, filtered over a Buchner funnel, and washed with 2 L of distilled water for each 3 g of material to remove adsorbed chloride, nitrate, and ammonium ions. Finally, the resulting wet solid was dried at 120 °C overnight and calcined at 750 °C for 3 h with a heating rate of 5 °C/min.

Cu was deposited on the supports by incipient wetness impregnation (IWI). A suitable amount of copper nitrate $Cu(NO_3)_2{\cdot}2.5H_2O$ was dissolved in a volume of water equivalent to the pore volume of the support, in order to reach the desired Cu loading on the final material. To guarantee a homogeneous distribution of metal, the solution was added dropwise to the support while stirring, until mud point (complete filling of pores) was reached. The powders were then oven dried and calcined at 450 °C for 5 h with a heating ramp of 2 °C/min.

Before testing, catalysts were formed in pellets with a granulometry between 20 and 40 mesh. To do so, the powder was pressed into a self-sustaining disk (~1 mm in height and 3 cm in diameter), which was then crushed using appropriate sieves.

To obtain a metallic Cu active phase on the catalysts surface, the calcined samples were reduced into the reactor system under 30 mL/min H_2 flow at 350 °C for 3 hours. In particular, the catalyst was heated at 10 °C/min under 30 mL/min of He up to 250 °C, then the flow was progressively switched to 30 mL/min of hydrogen (ca. 10 minutes wait), then the sample was heated in H_2 up to 350 °C at 10 °C/min, the final temperature was kept for 3 h.

2.2. Catalyst characterization

The XRD powder patterns of all materials were acquired using a Philips X'Pert diffractometer with Bragg-Brentano geometry, equipped with a pulse height analyzer and a secondary curved graphite-crystal monochromator. The specific surface area of the catalysts was determined with the BET method by N_2 absorption−desorption at liquid N_2 temperature using a Sorpty 1750 Fison instrument.

Temperature programmed desorption (TPD) of NH_3 and CO_2 was carried out with a Micromeritics Autochem II 2920 instrument coupled with a TCD detector and a Cirrus 2 quadrupole mass spectrometer to measure the total acidity and basicity of the materials. H_2-temperature-programmed reduction (H_2-TPR) was performed on a Micromeritics Autochem II 2920 instrument equipped with a TCD detector. SEM-EDS images for morphological and structural characterization were recorded using an EVO50 series instrument (LEO ZEISS) equipped with an INCAEnergy350 EDS microanalysis system and INCASmartMap (Oxford Instruments Analytical) for the elemental mapping. A TEM/STEM FEI TECNAI F20 microscope (Thermo Fisher Scientific, Waltham, MA, USA) equipped with an EDX analyzer and a HAADF (annular dark-field detector) was utilized for the high-resolution transmission electron microscopy (HRTEM) characterization.

For the determination of the La-Zr ratio in La-Zr-O, samples were analyzed with an Agilent 4100 MP-AES: microwave plasma-atomic emission spectrometer. Lanthanum content was determined at 394.910, 408.672 and 433.374 nm while Zirconium content was determined at 339.198, 343.823 and 349.621 nm. TGA analyses of spent catalysts were performed on a SDT Q 600 instrument, in order to identify the amount of heavy compounds absorbed on the catalyst surface. Raman spectroscopy analyses of the spent catalysts were carried out on a Renishaw RM1000 instrument (Renishaw plc, Wotton-under-Edge, UK), equipped with a Leica DM LM confocal microscope, video camera, CCD detector, and a green laser source Argon ion (514.5 nm).

2.3. Catalytic tests

The catalytic tests were carried out in a gas phase continuous-flow reaction system working at atmospheric pressure (Scheme S1 in the ESI). The inlet gas feed composition was maintained at 10 mol% EtOH in He (90 mol%). Liquid ethanol was fed by means of a high precision infusion pump (KPS 100 Syringe Pump) into a stainless-steel heated line to obtain instant vaporization and mixing with the carrier gas (He) which flows in the system. The heated line was connected with a tubular quartz reactor (length 600 mm, inner diameter 11 mm) containing the catalyst and placed inside a furnace.

The contact time τ (s) was set at the desired value and was calculated as the ratio between the volume of the catalyst loaded in the reactor (mL) and the total volumetric gas flow (mL/min) at the related reaction temperature:

$$\tau = \frac{V_{Catalyst}}{\dot{V}_{Total}} \times 60$$

The heavier products exiting the reactor were condensed in a trap kept at 25 °C and connected to the bottom of the reactor. The trap was changed at regular intervals of time and the liquid blends were analyzed by manual injection into an Agilent Technologies 6890 gas-chromatographer equipped with an Agilent HP-5 capillary column (30 m × 250 μm × 0.25 μm) and coupled with an Agilent Technologies 5973 mass analyzer (GC-MS).

The gaseous stream exiting the cold trap and rich in lighter uncon-

densed products was driven through a heated line to an on-line Agilent 6890 A gas-chromatograph. The instrument was supplied with two different columns, both connected to a dedicated TCD detector. CO_2 and ethylene were analyzed using a HP-PLOT-Q (30 m × 0.32 mm × 20 μm, total flow 1.4 mL/min) column, while the heavier uncondensed products (namely alcohols, aldehydes, ketones, higher alkanes and alkenes, phenolics and aromatics) were quantified using a DB-1701 (30 m × 0.53 mm × 1 μm, total flow 1.6 mL/min) column. Conversion (X%), yield (Y%), selectivity (S%) of the calibrated compounds and carbon balance (%) were calculated as follows:

$$X\% = \frac{n^{in}_{EtOH} - n^{out}_{EtOH}}{n^{in}_{EtOH}} \times 100$$

$$Y\% = \frac{\text{Carbon number}_{Product} \bullet n^{out}_{Product}}{\text{Carbon number}_{EtOH} \bullet n^{in}_{EtOH}} \times 100$$

$$S\% = \frac{Y_{Product}}{X} \times 100$$

$$\text{Carbon balance}\left(\sum Y \Big/ X\%\right) = \frac{\sum_i Y_i}{X} \times 100$$

3. Results and discussion

3.1. Catalyst characterization

The main physicochemical features of the supports (i.e., specific surface area, density of both acidic and basic sites and, if consistent with the material, La/Zr atomic ratio) are summarized in Table 1. The densities of acidic and basic sites reported in Table 1 are expressed as μmol/m^2 to allow an easier comparison of the intrinsic acidity and basicity of materials despite their different SSA.

The analysis of the TPD profiles of *t*-ZrO_2, *m*-ZrO_2, La-Zr-O and La_2O_3, Figs. S1–S8 in the ESI, showed that the density of basic sites, expressed as μmol/m^2 of desorbed CO_2, for these materials followed the order La_2O_3 (6.3 μmol/m^2) > *m*-ZrO_2 (4.3 μmol/m^2) > La-Zr-O (2 μmol/m^2) > *t*-ZrO_2 (0.8 μmol/m^2). Furthermore, while *m*-ZrO_2 and La-Zr-O possessed both weak and medium-strength basic sites (with desorption temperature of roughly 130 and 270 °C respectively), only weak sites were observed for *t*-ZrO_2 (with a desorption temperature of 125 °C). La_2O_3 had the highest density and strength of basic sites (max desorption temperature of 500 °C) but showed negligible acidity. It consisted of a pure hexagonal phase with high crystallinity (Figure S9 in the ESI). For the two crystalline phases of ZrO_2, CO_2 adsorption capacity of the monoclinic phase was higher than that of tetragonal phase, as previously observed by Pokrovski et al. [60]. This is due to the different atomic coordination of surficial atoms, which is lower for the monoclinic phase, since Zr^{4+} is heptacoordinated and not octacoordinated. XRD analysis of La-Zr-O showed that the material had a high degree of amorphism. Broad diffraction peaks of a poorly crystalline structure were observed, but they could be ascribed both to a tetragonal and a monoclinic phase (Figure S9).

The substitution of Zr with La, which is less electronegative, should leave higher electron density over the oxygen along the metal-oxygen bond, giving the O^{2-} anion a stronger base character and therefore increasing the CO_2 adsorption capacity of the mixed oxide La-Zr-O compared to ZrO_2, which is only true when La-Zr-O is compared to *t*-ZrO_2, which shows less basicity, while *m*-ZrO_2 is the most basic amongst the three materials. This evidence suggests that, even though the introduction of La in the structure decreased the degree of crystallinity, the elements involved in La-Zr-O were arranged in a tetragonal structure. The less electronegative La also provides less Lewis acidity, which is reflected in the lower NH_3 uptake. In fact, while acidity was quite similar between the two phases of zirconia, settling at 2.3 and 2.2 μmol/m^2 for *t*-ZrO_2 and *m*-ZrO_2, respectively, La-Zr-O showed a slightly lower density of acidic sites (1.5 μmol/m^2). NH_3 broad desorption peaks of the three supports indicated that weak, medium-strength and strong acidic sites are present on the surfaces, although the shift to lower temperatures for La-Zr-O showed that its acidic sites settle at an averagely lower strength.

The main physicochemical features of the catalyst after functionalization with Cu (specific surface area, actual Cu loading, reducibility of supported Cu) are summarized in Table 2. Metal loadings of 1 wt%, 5 wt% and 10 wt% were obtained on *t*-ZrO_2, leading to 1Cu/*t*-ZrO_2, 5Cu/*t*-ZrO_2 and 10Cu/*t*-ZrO_2 samples, respectively. Since 5 wt% resulted the best performing metal loading, only 5Cu/*m*-ZrO_2, 5Cu/La-Zr-O and 5Cu/La_2O_3 were synthesized.

After the final IWI step of copper deposition, followed by calcination, a dispersion of CuO was expected to be found on the catalysts surface. For 5Cu/*t*-ZrO_2 and 5Cu/*m*-ZrO_2, XRD analysis could not confirm the nature of the copper phase obtained, since the amount and the small size of the particles obtained did not produce any characteristic reflections in the diffractograms, which appeared identical to those of the unmodified supports (Figs. S10 and S11 in the ESI, respectively). On the contrary, 5Cu/La-Zr-O showed Bragg signals of CuO (Figure S12 in the ESI). XRD of 5Cu/La_2O_3 revealed that the impregnation process of La_2O_3 with Cu partially dissolved the support leading to its amorphization, as also suggested by the increased SSA from 27 m^2/g for La_2O_3 to 45 m^2/g for 5Cu/La_2O_3. At the same time, a $La_2O_2(CO_3)$ phase rose after IWI (Figure S13 in the ESI). Such phase could have been eliminated by calcination at 750 °C [61], but this would have led to major sintering of the supported Cu nanoparticles, therefore it was avoided. A study on

Table 1
Physicochemical features of the supports.

Support	BET SSA[a] (m^2/g)	La/Zr atomic ratio		Density of acidic sites[d] (μmol NH_3/m^2) (Desorption T (°C))	Density of basic sites[e] (μmol CO_2/m^2) (Desorption T (°C))
		MP-AES[b]	SEM-EDS[c]		
t-ZrO_2	153	-		2.3 (290)	0.8 (125)
m-ZrO_2	87	-		2.2 (300)	4.3 (130; 270)
La-Zr-O	256	0.26	0.28	1.5 (265)	2 (135; 270)
La_2O_3	27	-		0	6.3 (100; 250; 500)

[a] N_2 physisorption.
[b] Microwave plasma-atomic emission spectrometer.
[c] Scanning electron microscopy- energy-dispersive spectrometry.
[d] Ammonia temperature programmed desorption.
[e] Carbon dioxide temperature programmed desorption.

Table 2
Physicochemical features of Cu based catalysts[a].

Catalyst	BET SSA[b] (m^2/g)	Cu loading[c] (wt%)	H_2 consumption[d] (μmol/g) (Reduction T (°C))	Cu reduction degree[e] (%)
1Cu/*t*-ZrO_2	110	0.97	n.d.	n.d.
5Cu/*t*-ZrO_2	126	5.4	482 (157)	62
10Cu/*t*-ZrO_2	116	9.7	n.d.	n.d.
5Cu/*m*-ZrO_2	71	3.8	444 (128; 156; 216; 243)	57
5Cu/La-Zr-O	172	5.7	576 (191)	74
5Cu/La_2O_3	45	4.4	644 (290)	83

[a] n.d. = not determined.
[b] N_2 physisorption.
[c] Scanning electron microscopy-energy-dispersive spectrometry (SEM-EDS).
[d] H_2 temperature-programmed reduction.
[e] Calculated from the TPR results as: Measured H_2 consumption·100/Theoretical H_2 consumption (theoretical consumption for 5%wt of Cu: 777 μmol/g).

reducibility of CuO to Cu was performed to better understand copper dispersion and its interaction with the supports, and to identify the ideal conditions for *in-situ* reduction of the copper phase prior to reaction. TPR analyses on the Cu based catalysts (Figs S13–S17 in the ESI) revealed that the reduction of available copper on the surface of the supports took place with a temperature trend of 5Cu/La_2O_3 (290 °C) > 5Cu/*m*-ZrO_2 (T_{max} = 243 °C) > 5Cu/La-Zr-O (191 °C) > 5Cu/*t*-ZrO_2 (157 °C). However, while 5Cu/*t*-ZrO_2, 5Cu/La-Zr-O and 5Cu/La_2O_3 showed moderately sharp, single reduction peaks, 5Cu/*m*-ZrO_2 showed 4 reduction peaks centered at 128, 156, 216 and 243 °C, of decreasing intensity with increasing temperature. This implied that while copper was homogeneously dispersed on *t*-ZrO_2, La-Zr-O and La_2O_3, copper species and particles with different granulometries and crystallinity were found on the surface of *m*-ZrO_2 [62]. The similarity of interaction between Cu and the two supports 5Cu/*t*-ZrO_2 and 5Cu/La-Zr-O, deductible by the analogous peak shapes, could be ascribed to the fact that both supports have a tetragonal lattice coordination, as previously explained. Literature reports that small, well dispersed particles characterized by a strong interaction with the support show low reduction degrees and high reduction temperatures, suggesting that they are less easily reduced than bigger particles [63,64]. However, we noticed a positive correlation between reduction degree and reduction temperature for the catalysts reported in this work (Fig. 1), indicating that a strong interaction between the metal oxide particles and the support is linked to a better reducibility of CuO in our case.

An accurate statistical distribution of particle size by TEM analysis on this kind of catalysts is challenging, due to the relatively high electron density of Zr and La, which do not allow for an optimal imaging contrast with Cu. Compatibly to experimental limitations, the average CuO particle size on the different supports is also shown in Fig. 1.

3.2. Catalytic tests

3.2.1. Catalytic activity of Cu/*t*-ZrO_2: influence of Cu loading

At first, the effect of Cu loading was studied. Fig. 2 summarizes the outcome of different tests carried out on 1Cu/*t*-ZrO_2, 5Cu/*t*-ZrO_2 and 10Cu/*t*-ZrO_2, as histograms representing the compounds found in the outlet flow at 2 h of time on stream. The same reaction was carried out on the unmodified support *t*-ZrO_2 for reference. Tests were carried out in the gas phase at 300 °C, with a percentage of EtOH in the feed stream equal to 10 mol% in He, and a contact time (τ) of 2 s. Reactions were preceded by reduction of the copper phase under a flow of H_2 at 350 °C for 3 h. For unmodified *t*-ZrO_2, the catalyst was pretreated under a He flow at 300 °C for 1 h before starting the EtOH feed. Results of the tests are expressed in terms of conversion of EtOH (X EtOH), products selectivity (S) and molar balance, calculated as the sum of yields divided by conversion (ΣY/X). The catalytic test over unmodified *t*-ZrO_2 (white bar in the histogram) showed low EtOH conversion with the formation

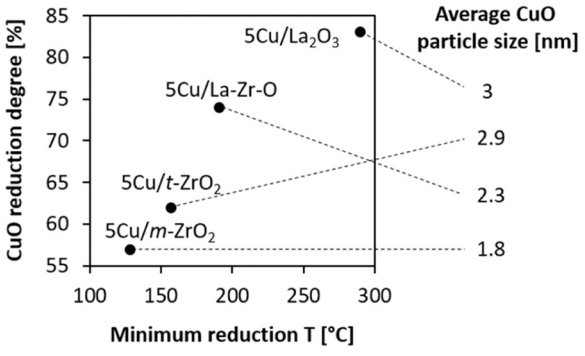

Fig. 1. Correlation between reduction degree and minimum reduction temperature of CuO in the catalysts. On the right, average CuO particle size on the different supports obtained by TEM analysis.

of products mainly derived from acid catalyzed condensation and dehydration, such as diethyl ether and ethylene. Acetaldehyde was observed, suggesting a limited but existing ability by the basic sites of *t*-ZrO_2 to perform hydrogen transfer, as also recently confirmed by our group [57]. Aldol condensation of acetaldehyde and subsequent dehydrogenation gave minor selectivity in 1-butanol through a Guerbet mechanism [65]. Butadiene was also observed as a product of Ostromislenski and/or Lebedev reactions [66,67].

Upon introduction of copper on the surface of the catalyst, a variety of products was identified in the outlet stream. EtOH conversion was boosted from 20%, obtained on the unmodified support, to a minimum of 70% with the lowest Cu loading of 1 wt% (1Cu/*t*-ZrO_2), while it reached 90 and 93% with 5Cu/*t*-ZrO_2 and 10Cu/*t*-ZrO_2, respectively. Acetaldehyde was the most abundant compound with a selectivity ranging from 27% to 30%. A few light compounds with a carbon number between three and five were observed. The presence of crotonaldehyde and its hydrogenated analogue butyraldehyde, typical products of the condensation of acetaldehyde, corroborated the existence of a Guerbet-like reaction pathway in which butyraldehyde is eventually transformed into 1-butanol through a final hydrogenation step. In fact, 1-butanol was found as a minor product and was therefore included in the <C6 others. Its low selectivity indicated either its homologation to higher alcohols through the same Guerbet path or its participation as an intermediate to other consecutive mechanisms (this will be further tackled later in this work). The observation of ethyl acetate and butyl butyrate, products of dehydrogenative coupling of ethanol and butanol [49,68] represented an example of alcohol conversion that could be promoted by the catalytic system. Such mechanism accounted for the low selectivity in 1-butanol. The production of acetone in the light fraction of the outlet stream can be explained as the outcome of ketonization of ethyl acetate [69]. Similarly, 2-pentanone is produced by ketonization of ethyl acetate with ethyl butyrate, the former being originated by dehydrogenative coupling of two molecules of EtOH and the latter by dehydrogenative coupling of 1-butanol and EtOH. The reiteration of such mechanisms on heavier molecules gave rise to a variety of compounds containing up to 14 carbon atoms, which were obtained over 5Cu/*t*-ZrO_2 with a significant selectivity of ca. 30% at 300 °C with only 2 s of contact time.

Since at such preliminary stage the attention was focused on the mere feasibility to reach a medium to high molecular weight suitable for processing in the jet fuel industry, all of the products containing 6 carbon atoms or more were gathered in the C6+ fraction for simplicity, since this fraction can possess the required properties previously described. However, it soon became necessary to operate a deeper analysis of the nature and properties of this fraction in order to maximize its production through wise adjustments of the catalytic system and conditions. As the best selectivity in heavy compounds was obtained over 5Cu/*t*-ZrO_2, Fig. 3 shows the composition of the C6+ fraction obtained with such catalyst in terms of molar fraction of each family of compounds normalized on the total of the C6+ fraction itself.

Ethyl butyrate was highlighted both due to its direct link to one of the main light products 2-pentanone and due to its lowest boiling point among the C6+ fraction. Examples of heavier esters mainly included butyl butyrate, ethyl hexanoate, ethyl 2-ethylbutyrate, ethyl 2-ethylhexanoate, but also butyl 2-ethylbutyrate and butyl octanoate were observed. Linear ketones, which formation has been explained, mainly included 2- and 4-heptanone, 2- and 4-nonanone, 4-undecanone, other than a minor quantity of 4-tridecanone. Amongst cyclic ketones, alkylated (namely ethyl-, methyl-, dimethyl-, trimethyl-, tetramethyl-) cyclohexanones and cyclohexenones were the main contributors. They were obtained by self-condensation of acetone or by condensation of the latter with crotonaldehyde [70,71]. Aromatics, in particular phenolics such as 2-ethyl-5-methylphenol, 5-isopropyl-2-methylphenol, 2-(*tert*-butyl)-3-methylphenol, could be obtained by progressive dehydrogenation of the aforementioned cyclic ketones. Regarding aromatic hydrocarbons, a Diels-Alder pathway, followed by dehydrogenation of

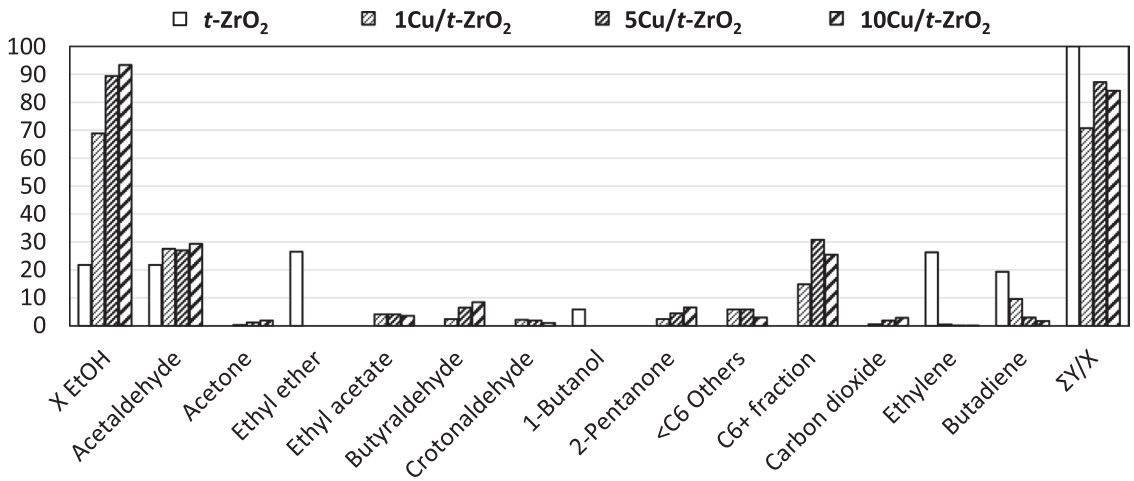

Fig. 2. Conversion of EtOH (X EtOH), molar balance (ΣY/X) and products selectivity (S) in ethanol upgrading over *t*-ZrO_2, 1Cu/*t*-ZrO_2, 5Cu/*t*-ZrO_2, 10Cu/*t*-ZrO_2. Reaction conditions T = 300 °C, τ = 2 s, EtOH 10 mol% in He.

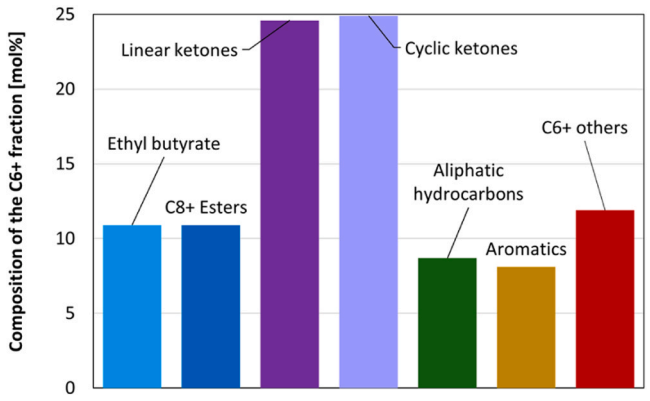

Fig. 3. Composition of the C6+ fraction expressed as molar fraction of each family of compounds normalized on the total of the C6+ fraction. Catalyst 5Cu/*t*-ZrO_2, reaction conditions T = 300 °C, τ = 2 s, EtOH 10% in He. Data obtained at 2 h of time on stream.

the intermediates, between butadiene with itself or ethylene was also considered, even though the formation of these olefins, and therefore their consumption in consecutive reactions, was low on a fresh catalyst. In fact, their selectivity increased with deactivation. Linear and, to a minor extent, cyclic aliphatic hydrocarbons (aliphatic HC, saturated and unsaturated) were also observed, most likely as products of alcohol dehydration. Scheme 4 shows an example of the aforementioned reaction paths leading to the main products observed. Due to the considerable number of compounds detected, the scheme cannot be considered exhaustive, but each reaction step can be taken as a model and applied to different intermediates. A more detailed scheme of the leading reactions promoted by our catalyst is reported in Scheme S2**.**

The fact that selectivity in acetaldehyde was similar for the three different Cu loadings while selectivity for C6+ products was highest at an intermediate Cu loading of 5 wt% (Fig. 2) could be explained with different reasonings while moving towards a lower or a higher Cu loading. In fact, since acetaldehyde is a primary product coming from the direct dehydrogenation of EtOH, its production seems to be efficient and fast enough to not be dramatically affected by the change in Cu content over the catalyst. On the contrary, its consumption occurred via a complex scheme of consecutive reactions which seemed to behave as rate determining step affecting not only acetaldehyde transformation but the overall process productivity towards long-chain compounds. These consecutive reactions of acetaldehyde (i.e., aldol condensations or ester formation via Tischenko-like reactions) usually take place on the active sites of *t*-ZrO_2 (basic and acidic sites, respectively).

It is likely that the acetaldehyde molecules that exhibit the highest reactivity are those still in close proximity to copper, as they are more easily adsorbed onto the metal oxide surface than those that are desorbed into the bulk gaseous phase. Therefore, a crucial role is played by the interface between the metal and the oxidic support, which not only enhances the direct DHC of ethanol but also the previously explained consecutive reactions of adsorbed acetaldehyde.

3.2.2. *Catalyst deactivation*

Conversion and selectivity of the main products were plotted as a function of the time on stream to reveal the deactivation of the catalytic system over time, given by the progressive change in product distribution (Fig. 4).

It is important to note that deactivation could be observed both in the decrease of EtOH conversion and in the increase of selectivity in acetaldehyde and other lighter products at the expenses of the C6+ fraction, and the two events did not happen with the same rate. Accordingly, we identified different possible causes for the two phenomena, such as a progressive reoxidation of Cu to CuO and the physical deposition of coke on the catalyst surface blocking the active sites. As a matter of fact, conversion of EtOH is mainly linked to the efficiency of dehydrogenation and dehydrogenative coupling leading to acetaldehyde and ethyl acetate, respectively. These reactions are promoted by copper, thus it is legitimate to imagine that a change in the nature of the copper phase could decrease the ability of the system to transform EtOH. At the same time, dehydrogenation and dehydrogenative coupling are important steps of the cascade reaction scheme on heavier intermediates, hence a shift to lower molecular weights with an increase of acetaldehyde selectivity can be expected to be a consequence as well. Comparison between selectivity in acetaldehyde, C6+ fraction and EtOH conversion for catalysts 5Cu/t-ZrO_2 and 5CuO/t-ZrO_2, the latter being tested without reducing the copper phase prior to reaction, is shown in Table 3. At the same time on stream of 2 h and compared to Cu, CuO gave a lower conversion while showing a higher selectivity for acetaldehyde and a lower ability to promote the cascade reaction scheme we proposed. Therefore, it is likely that a transformation of Cu into CuO during reaction would give a similar effect of progressive decrease of conversion and molecular weight in the reaction products, which was precisely what we observed in Fig. 4.

A study on the effect of contact time proved helpful in understanding the deactivation process. Catalytic results obtained with contact times of 1 and 3 s were thoroughly analyzed and compared to those obtained at 2 s in the ESI (Figure S18), while only the relevant information is

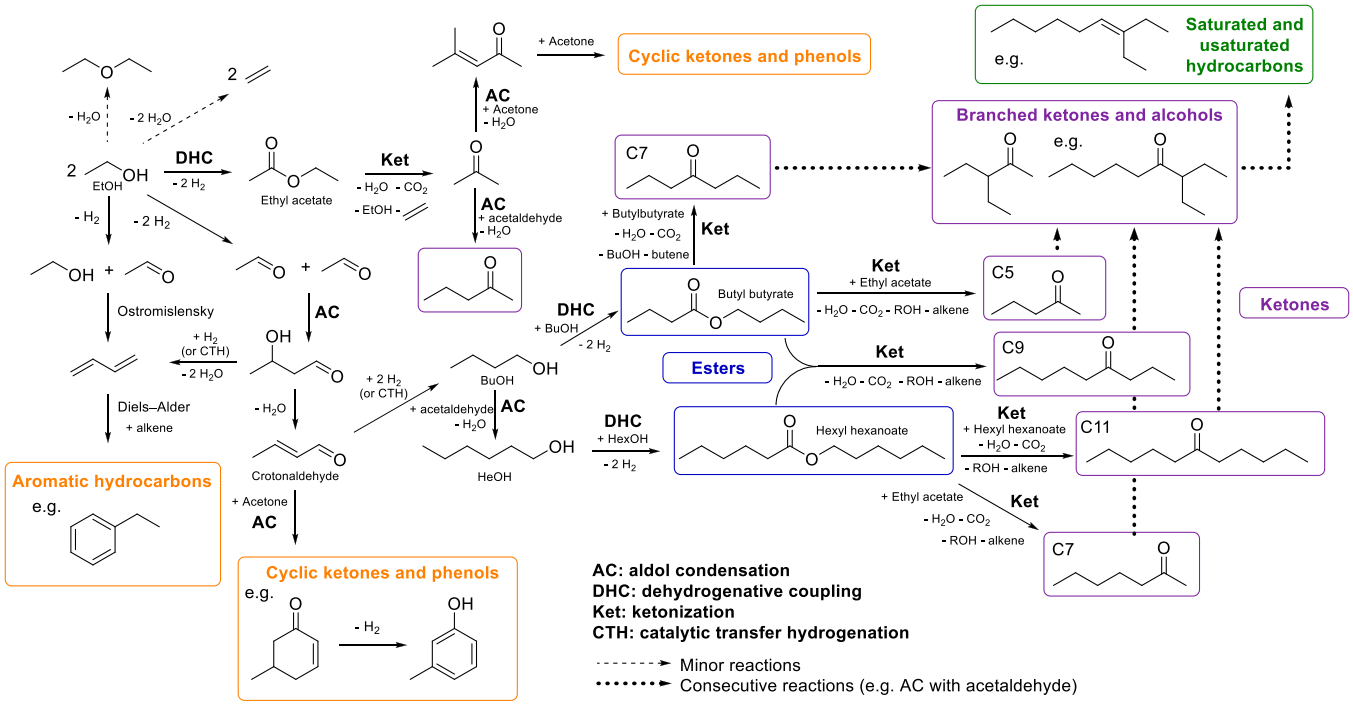

Scheme 4. Cascade reaction scheme leading to the main products observed.

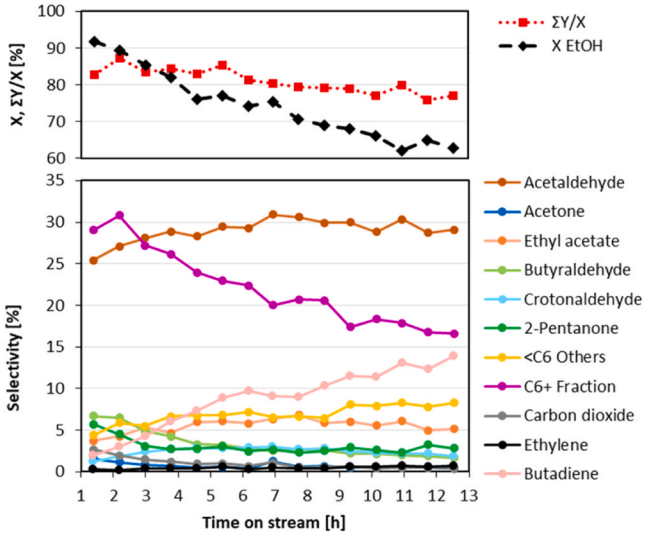

Fig. 4. Conversion of EtOH (X EtOH), molar balance (ΣY/X) and products selectivity (S) as a function of time on stream over catalyst 5Cu/*t*-ZrO_2. Reaction conditions T = 300 °C, EtOH 10% in He.

Table 3
EtOH conversion, acetaldehyde and C6+ fraction selectivity over 5Cu/*t*-ZrO_2 and 5CuO/*t*-ZrO_2. Reaction conditions T = 300 °C, EtOH 10% in He, τ = 2 s, time on stream = 2 h.

Compound or fraction (X, S %)	5Cu/*t*-ZrO_2	5CuO/*t*-ZrO_2
EtOH	90	72
Acetaldehyde	27	46
C6+ fraction	31	24

discussed herein. In general, increasing the contact time led to a more stable EtOH conversion accompanied by a lower concentration of acetaldehyde amongst the reaction products, showing a qualitative connection between the two parameters. Fig. 5, top, shows an overlap of EtOH conversion and acetaldehyde trends throughout the three contact times. Fig. 5, bottom, shows average EtOH conversion plotted as a function of average acetaldehyde selectivity (the average was calculated over the range 1–13 h of time on stream), revealing the inverse correlation between stability of the catalyst (higher average EtOH conversion) and acetaldehyde concentration in the reaction mixture. It appeared that the lower the contact time, the less the dehydrogenated intermediate was further converted into the products of interest and this could give rise to decarbonylation, decarboxylation and polycondensation of acetaldehyde, which had been proven responsible for coke formation over catalysts bearing Lewis or Brønsted acid sites [72].

The presence of carbonaceous material on the surface of the spent catalyst was confirmed by TGA and Raman spectroscopy. FT-IR/ATR analyses were performed to collect more details on the adsorbed species, but their identification resulted challenging. TGA (Fig. 6, top) conducted in air showed an abrupt weight loss starting at 220 °C, with a slope change around 310 °C, demonstrating that the existence of different types of carbon deposits was likely. Typical D-band and G-band of amorphous and crystalline coke, respectively, were observed by Raman spectroscopy (Fig. 6, bottom) [73]. A notable aspect is the 0.23% weight increment occurring around 140 °C, which was attributed to the reoxidation of roughly 19% of the supported Cu to CuO. On the other hand, an accumulation of 5.1 wt% of carbonaceous residue corresponds to the loss of around 4% of the EtOH fed to the catalyst, considering the adsorbed species as graphene.

XRD of the fresh and spent catalyst did not show visible sintering of Cu particles, since no Cu or CuO Bragg signals were visible in the spent diffractogram, and the phase resulted stable throughout the entire reaction with no change in phase whatsoever (Figure S10 in the ESI). Widespread sintering phenomena were also excluded thanks to TEM images of fresh and spent 5Cu/*t*-ZrO_2 (Fig. 7). The observed Cu nanoparticles fell in a range between 1.2 and 5 nm, and their size did not show diffuse increase after reaction, except for rare localized bigger agglomerates. On the other hand, the nitrogen physisorption characterisation of the spent materials (Table S1) confirms a general trend in losing between 20% and 30% of the specific surface area during the catalytic test, again proving the fouling of the surface with heavy

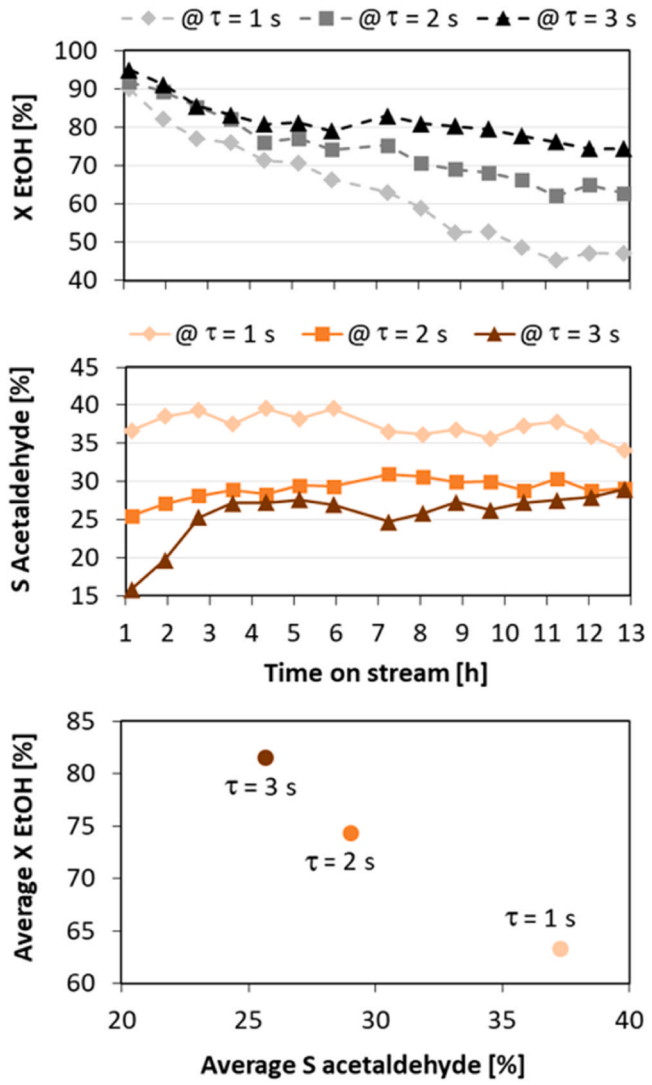

Fig. 5. Top left, overlap of EtOH conversions over 5Cu/*t*-ZrO_2 for τ = 1, 2 and 3 s. Bottom left, overlap of Acetaldehyde selectivities over 5Cu/*t*-ZrO_2 for τ = 1, 2 and 3 s. Right, correlation between average EtOH conversion and Average acetaldehyde selectivity for the different contact times.

organic compounds. The only exception is 5Cu/La_2O_3 that shows a loss of around 50% of SSA probably due to both fouling and carbonation and hydration of the surface.

3.2.3. *Physicochemical analysis of the C6+ fraction*

Aside from deactivation, which we set the objective to tackle later by modifying the catalytic system and/or the reaction conditions, these screening tests proved encouraging in terms of selectivity for medium-heavy compounds, especially using 5Cu/*t*-ZrO_2 with a τ = 2 s, therefore we commissioned a physicochemical analysis of the C6+ fraction. A mixture was prepared using around 20 different commercial equivalents or isomers (Table S2 in the ESI) of the main compounds detected in the C6+ fraction and the final blend was sent to SGS Italia S.p.A.; Oil, Gas and Chemicals (Genoa, Italy) for analysis. Results are shown in Table 4.

Comparison between our test blend and the ASTM D1655 Standard showed promising results, with almost all parameters falling close to the requirements. As the least fitting entry, the aromatic content resulted around 40% higher than the maximum threshold, while the naphthalene equivalents met the specification. Slightly low gross heat of combustion [74] and high density compared to the standard specification suggested that the compounds might have been too oxygen rich and the production

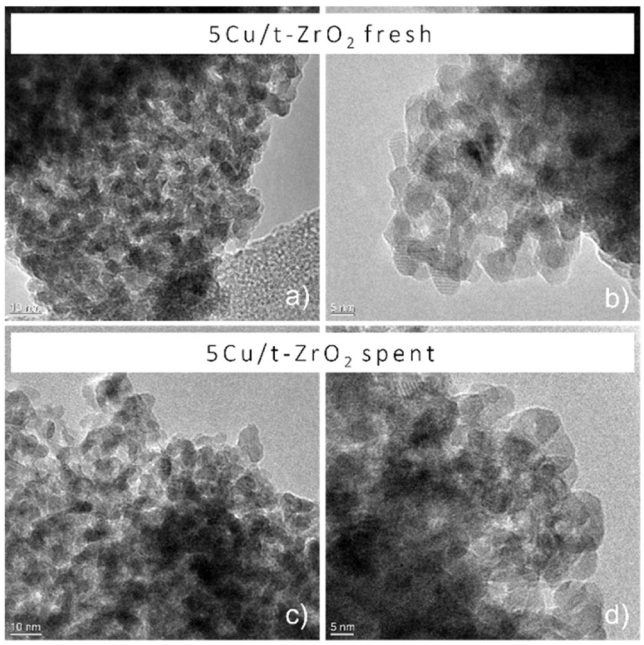

Fig. 6. TEM images of 5Cu/t-ZrO_2. a) and b), fresh catalyst; c) and d), spent catalyst after reaction at τ = 2 s.

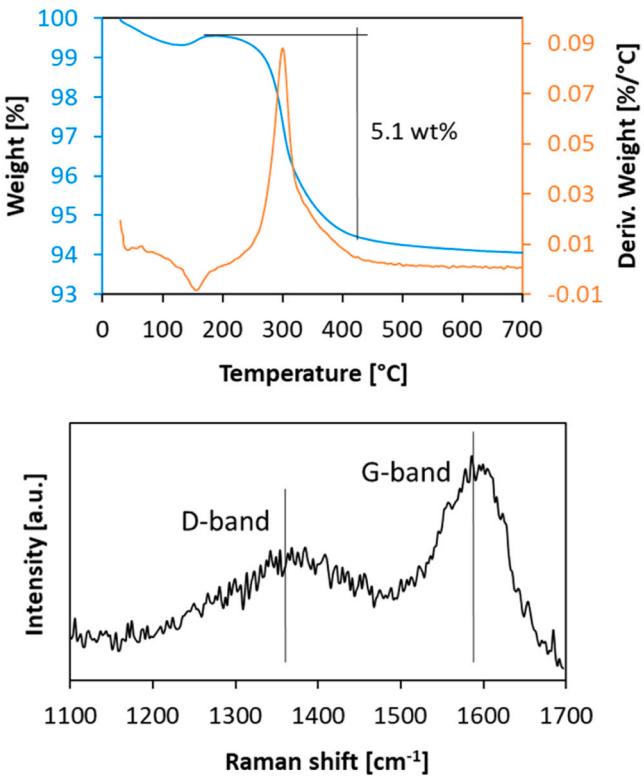

Fig. 7. Characterization of spent catalyst 5Cu/*t*-ZrO_2 after reaction at τ = 2 s. Top, TGA analysis in air. Bottom, Raman spectroscopy analysis.

of more dense and oxygenated compounds such as esters should have been minimized. Flash point and freezing point fell around 10% out of range.

3.2.4. *Catalytic activity of 5Cu/t-ZrO_2 with co-feeding of H_2*

Based on the information collected during the preliminary optimization of the catalytic system and reaction conditions as well as upon the

Table 4
Properties of the C6+ fraction compared to ASTM D1655 Standard.

Property	C6+ fraction	ASTM D1655 Standard
Aromatics	36%	< 25%
Density	865 kg/m^3	775–840 kg/m^3
Gross Heat of Combustion	37.7 MJ/kg	> 42.8 MJ/kg
Naphtalene	0.93%	< 3%
Flash point	34 °C	> 38 °C
Sulphur	0%	< 0.3%
Freezing point	-36.5 °C	< −40 °C (Jet A) / < −47 °C (Jet A-1)

physicochemical analysis on the test blend, the main goals for the subsequent tests were identified as: i) to control and mitigate deactivation, ii) to increase selectivity for C6+ fraction at the cost of acetaldehyde, iii) to reduce the aromatic fraction and iv) to modulate the composition in order to comply with the required standards.

We tried assessing the possibility to increase the catalyst lifetime by co-feeding molecular hydrogen during reaction. The beneficial effect of H_2 could consist of both keeping Cu at a reduced form and operating a progressive cleansing of the catalyst surface from the deposited material throughout the course of the reaction.

Fig. 8 displays the results of diluting EtOH in a mixture of He and H_2 in a 1:1 ratio by keeping all the reaction system at atmospheric pressure. Even though conversion still underwent a decline from 95% to 88% in 13 h, selectivity in the heavy fraction remained steady at around 40% during the entire reaction time. It is worth observing that this happened despite the contemporary increase in selectivity for acetaldehyde from 14% to 22%, which did not happen at the expense of C6+ fraction selectivity but due to the decrease in selectivity for ketonization light products such as acetone, 2-pentanone and CO_2. It could be assumed that, in this case, a partial deactivation of the active sites responsible for aldol condensation (limiting step of the reaction mechanism) did not correspond to a deactivation of the dehydrogenative coupling ability of the system, a key step to C6+ molecules. This highly suggested that while the re-oxidation of Cu was successfully avoided by co-feeding H_2, the physical blockage of the active sites of the support due to coking and/or deposition of heavy compounds was still happening to some extent. No crotonaldehyde build up was observed, which could be attributed to activation of molecular hydrogen in the reaction conditions. For this reason, the absence of butadiene suggested that its preferred formation mechanism may have been through the Ostromislensky path instead of hydrogenation and consecutive dehydration of crotonaldehyde. Noticeably, few cyclic ketones, namely alkylated cyclohexenones and cyclohexanones, and no aromatics were detected. Crossing this information with the absence of crotonaldehyde in the outlet stream and interpreting the result according to Scheme 4, the reaction path of formation of cyclohexenones from self-condensation of acetone and/or condensation of acetone with crotonaldehyde, followed by dehydrogenation to phenols found validation. A similar reasoning could be carried out for the absence of aromatic hydrocarbons, the production of which from Diels-Alder of butadiene and other alkenes might be confirmed by the low selectivity for butadiene observed in Fig. 8. It is evident that the presence of a partial pressure of only 0.45 atm of H_2 in the reaction environment barely affected the equilibria through Le Chatelier principle, as reactions producing hydrogen, most notably dehydrogenation of EtOH to acetaldehyde, seemed taking place undisturbed. The detailed analysis of the C6+ fraction constituents revealed that, although the overall selectivity for heavy molecules was retained, a progressive change in composition was observed, confirming that absolute stability of the catalyst was not achieved. Ketones were the main components, settling between 52% and 61% during the first 6 h, before slowly decreasing in abundance. All esters contributed to a quite stable 12% during the first 6 h, followed by an increase ascribable to the deactivation of the sites responsible for ketonization reactions. Aliphatic hydrocarbons contributed as a minor fraction.

3.2.5. *Catalytic activity of copper over different Zr and La oxides*

Co-feeding H_2 successfully helped to improve the selectivity in the desired product mixture and hindered deactivation. However, the use of hydrogen on a large scale presents safety concerns, not to mention the high costs related to the technologies required. Moreover, the sustainability of the entire process would be compromised in case fossil hydrogen was employed. For these reasons, we thought of circumventing the use of molecular hydrogen, while still obtaining analogous positive effects, by tuning the properties of the non-innocent support.

Previous work by De Maron et al. demonstrated a superior activity of *m*-ZrO_2 over *t*-ZrO_2 for the ketonization of propionic acid, attributing such phenomenon to a higher density of basic sites on *m*-ZrO_2 compared to *t*-ZrO_2 [54]. As ketonization is one of the main reaction mechanisms in our system, we hypothesized that enhancing this step could shift the equilibria towards higher molecular weights, lowering selectivity for acetaldehyde and thus containing deactivation. Therefore, we

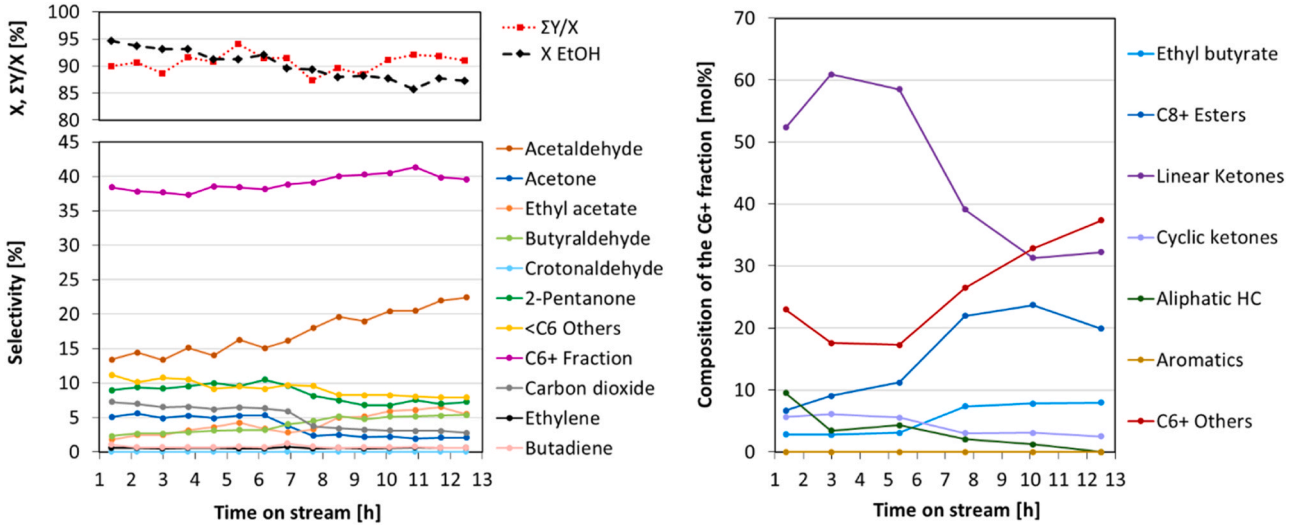

Fig. 8. Left, Conversion of EtOH (X EtOH), molar balance (ΣY/X) and products selectivity (S) as a function of time on stream over catalyst 5Cu/*t*-ZrO_2. Right, Composition of the C6+ fraction expressed as molar fraction of each family of compounds normalized on the total of the C6+ fraction, as a function of time on stream. Reaction conditions T = 300 °C, τ = 2 s, EtOH 10% in a carrier gas mixture composed of He and H_2 in a 1:1 ratio.

synthesized 5Cu/*m*-ZrO_2 and tested it in our system.

The results are shown in Fig. 9, left hand-side, as a function of the time on stream. A test on the bare *m*-ZrO_2 support is reported as a reference in Figure S20 in the ESI.

The ketonization potential of *m*-ZrO_2 was confirmed. 2-Pentanone was initially detected with a selectivity of 25%, although with a decreasing trend. CO_2, a co-product of ketonization, was also observed in higher selectivity compared to previous tests. On the contrary, as expected, acetaldehyde selectivity was greatly reduced to less than 10% during the first two hours of time on stream, and its increase mirrored the decreased in ketonization products showing the link between the two trends. The overall improved selectivity for the C6+ fraction, reaching 35% and remaining above 30% after 6 h of reaction, corroborated the assumption that a more efficient catalyst in promoting ketonization reactions may lead to a progressive shift of the reaction equilibria towards heavier molecular weights.

The composition of the C6+ fraction (Fig. 9, right hand-side) swept away any doubts about the enhanced ketonization ability of the catalytic system, as the molar fraction of linear ketones settled around 80% during the first 2 h of reaction. The concomitant lack of aromatics and butadiene amongst the products of this catalytic test once again suggested the Diels-Alder mechanism.

The different effect of deactivation on catalyst activity and selectivity was observed. In fact, while conversion (and therefore catalyst activity) only decreased from 98% to 95% in around 6 h, acetaldehyde selectivity increased from 9% to 21%. C6+ fraction selectivity oscillated between 35% and 30% respectively, but its composition clearly showed a change over time, indicating a modification of the catalytic system similar to that observed in the case of co-feeding H_2 on 5Cu/*t*-ZrO_2. In particular, deactivation was associated with the concomitant selectivity decrease for ketones and increase for esters, the reactants of ketonization, which fact could be in agreement with a basic-site selective fouling (Fig. 9, right). In order to ultimately confirm that a more efficient ketonization was ascribable to a higher density and strength of basic sites on the support, a third material based on a La-Zr-O mixed oxide, characterized by an intermediate basicity, was synthesized *ad hoc* and compared with both *t*- and *m*ZrO_2 supports. The results obtained with 5Cu/La-Zr-O are reported in Fig. 10. For comparison, the catalytic results obtained over the bare support (La-Zr-O) are reported in Figure S21 in the ESI.

The behavior resulted similar to that of 5Cu/*m*-ZrO_2, even though ketonization was less effective due to the lower basicity of La-Zr-O compared to *m*-ZrO_2 (Table 1). Relatively high selectivity for 2-pentanone, CO_2 and C6+ fraction was accompanied by low selectivity for acetaldehyde at the beginning of the reaction, although a deactivation trend was still observed. Selectivity for the heavy fraction remained above 30% for the first 6 h of reaction, while conversion underwent a slight drop from 97% to 95%. Regarding the composition of the C6+ fraction, linear ketones were predominant (50% selectivity at 2 h) but lower in selectivity compared to those obtained with 5Cu/*m*-ZrO_2 (around 80%). Their selectivity remained relatively stable, indicating a lower deactivation of the basic sites promoting ketonization. Almost no aromatics were detected confirming the similarity of contribution of *m*-ZrO_2 and La-Zr-O to the reaction mechanism.

A trend of increasing ketonization efficiency with increasing basicity of the support was confirmed: Fig. 11 displays the molar fraction of ketones in the C6+ fraction at 2 h of time on stream as a function of the ratio between the density of basic sites and the density of acidic sites. On the other hand, the absence of acidic sites for La_2O_3 (as revealed by TPD analysis results in Table 1) caused the decrease of selectivity in C6+ fraction to less than 10% since the first hours of reaction (see Figure S22 in ESI), suggesting that a synergic effect of both acidic and basic sites is necessary for the development of the entire cascade reaction scheme. A dedicated chapter on 5Cu/La_2O_3 catalytic activity of the target process is reported in the ESI.

3.2.6. *Upgrading of 1-butanol over 5Cu/t-ZrO_2*

In order to validate the reaction mechanism proposed and observe the behavior of the catalytic system on a higher analogue of EtOH, 5Cu/*t*-ZrO_2 was tested for the upgrading of 1-butanol (BuOH). BuOH conversion was 90% during the first 2 h of time on stream and decreased to 82% after 6 h of reaction (Fig. 12, top left), showing a milder decrease compared to the parallel test conducted on EtOH (Fig. 4), where conversion at 6 h fell around 74%. This can be seen as validation that the reactant's conversion is affected by the deposition of coke or coke precursors, such as heavy adducts which can originate from polycondensation of acetaldehyde followed by decarbonylation, decarboxylation, as previously explained. In fact, butyraldehyde, which was the analogous observed product of acetaldehyde when BuOH was used as a reactant, is less reactive and therefore less prone to undergo such reactions, finally limiting the fouling of the catalytic surface. Moreover, the absence of acetaldehyde affected the aromatics production, which halved (Fig. 12, right vs Fig. 3). Ketonization appeared to be less efficient, probably due to the increasing length of the esters formed (C8 or longer) which limits their reactivity. It is important to note that

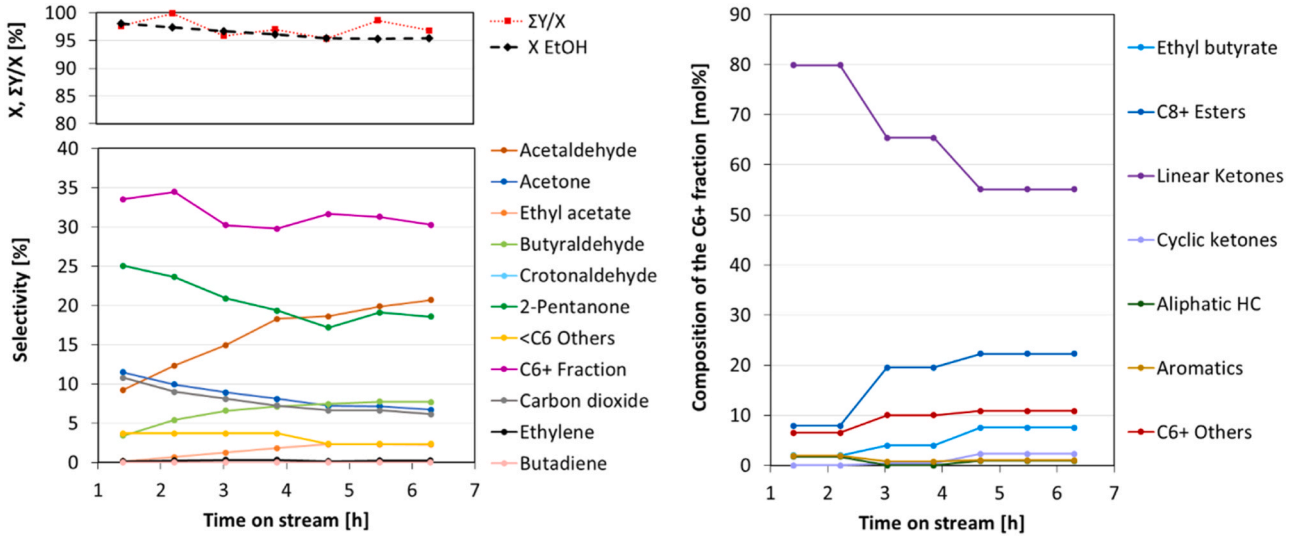

Fig. 9. Left, conversion of EtOH (X EtOH), molar balance (ΣY/X) and products selectivity (S) as a function of time on stream over catalyst 5Cu/*m*-ZrO_2. Reaction conditions T = 300 °C, τ = 2 s, EtOH 10% in He. Right, Composition of the C6+ fraction expressed as molar fraction of each family of compounds normalized on the total of the C6+ fraction, as a function of time on stream.

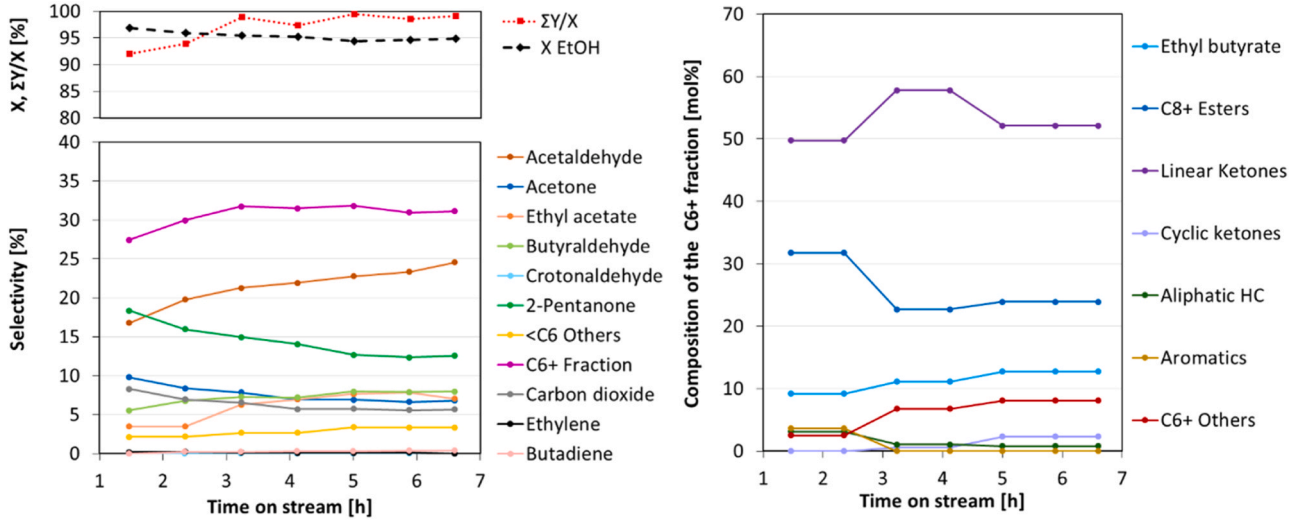

Fig. 10. Left, Conversion of EtOH (X EtOH), molar balance (ΣY/X) and products selectivity (S) as a function of time on stream over catalyst 5Cu/La-Zr-O. Reaction conditions T = 300 °C, τ = 2 s, EtOH 10% in He. Right, Composition of the C6+ fraction expressed as molar fraction of each family of compounds normalized on the total of the C6+ fraction, as a function of time on stream.

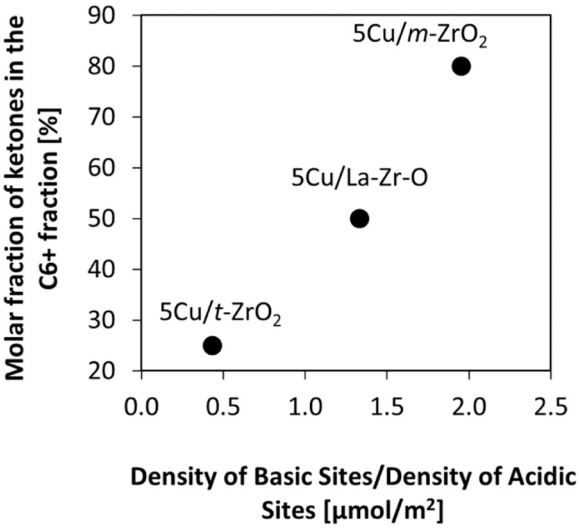

Fig. 11. Correlation between molar fraction of ketones observed at 2 h of time on stream and the ratio between density of basic sites and density of acidic sites, for the catalysts 5Cu/*t*-ZrO, 5Cu/*m*-ZrO_2 and 5Cu/La-Zr-O.

even though CO_2 selectivity seems low (around 1% at 2 h of time on stream) to support the ketonization mechanism, carbon numbers and stoichiometric coefficients must be considered (i.e., all yield are normalized considering the C atoms). While in fact a factor of 1/4 is involved when calculating CO_2 yield in the reactions starting from BuOH, a factor of at least 7/4 is used for ketone yields (lightest C7 ketones vs BuOH C4). Surprisingly, selectivity for aliphatic HC increased compared to EtOH test.

Overall, despite the lower reactivity of BuOH compared to EtOH, C6+ selectivity increased to a stable 50%, due to the higher carbon number of the reactant.

Since biobutanol can be obtained from the anaerobic fermentation of lignocellulosic biomass, just as bioethanol [75], the possibility to also feed BuOH to the catalytic system with good results definitely enhances its potentials and applicability.

4. Conclusions

The gas-phase, continuous flow catalytic upgrading of ethanol to heavier compounds in the jet fuel range was investigated. The employment of a relatively simple and cheap 5 wt% copper on tetragonal zirconia (5Cu/*t*-ZrO_2) multifunctional catalytic system allowed for the promotion of a complex one-pot reaction scheme relying on several cascade mechanisms. In particular, the reactions involved included alcohol dehydrogenation to aldehyde, alcohol direct coupling to esters through dehydrogenative coupling (DHC), ketonization, which can transform those esters into ketones, consecutive aldol condensation of esters/ketones with acetaldehyde and other longer aldehydes and catalytic transfer hydrogenation (CTH). This approach led to 90% ethanol conversion and 31% selectivity for a C6+ multicomponent blend featuring the presence of linear and branched esters, linear, branched and cyclic ketones, linear and branched alcohols and aldehydes, aromatics, phenolics and aliphatic hydrocarbons. The physicochemical analysis of a mixture of commercial analogues mirroring that obtained in a typical catalytic test showed a promising proximity to the properties of Jet A and A-1, which are the most diffused standards of jet fuel worldwide. However, acetaldehyde was found as the most abundant compound and its polymerization on the catalyst surface was suggested as a precursor of coke formation causing deactivation. Indeed, we found that limiting acetaldehyde selectivity helped limiting deactivation as well. It was also hypothesized that an additional cause of deactivation could be the progressive reoxidation of the active phase Cu to the less active CuO in the reaction conditions. The co-feeding of molecular hydrogen during the catalytic test proved to be an effective way to reduce such phenomenon and achieve a better control on the stability of the system, allowing for 40% C6+ fraction selectivity during the first 13 hours of time on stream, with conversion never falling below 85%. Similar results were obtained by modifying the non-innocent support. When using monoclinic zirconia as a support (5Cu/*m*-ZrO_2), the selectivity for the C6+ fraction was maintained between 35% and 30% during the first 6 hours of time on stream, with conversion above 95%. Analogous results were obtained upon the use of a mixed oxide support La-Zr-O, obtained by coprecipitation (5Cu/La-Zr-O). Characterization by CO_2 Temperature Programmed Desorption (TPD) of the supports revealed the following basicity trend: *m*-ZrO_2 > La-Zr-O > *t*-ZrO_2. In this regard, a positive correlation between the basicity of the catalyst and the molar fraction of ketones in the C6+ blend was observed. In fact, basic sites are key to ketonization, which is an important step in the cascade

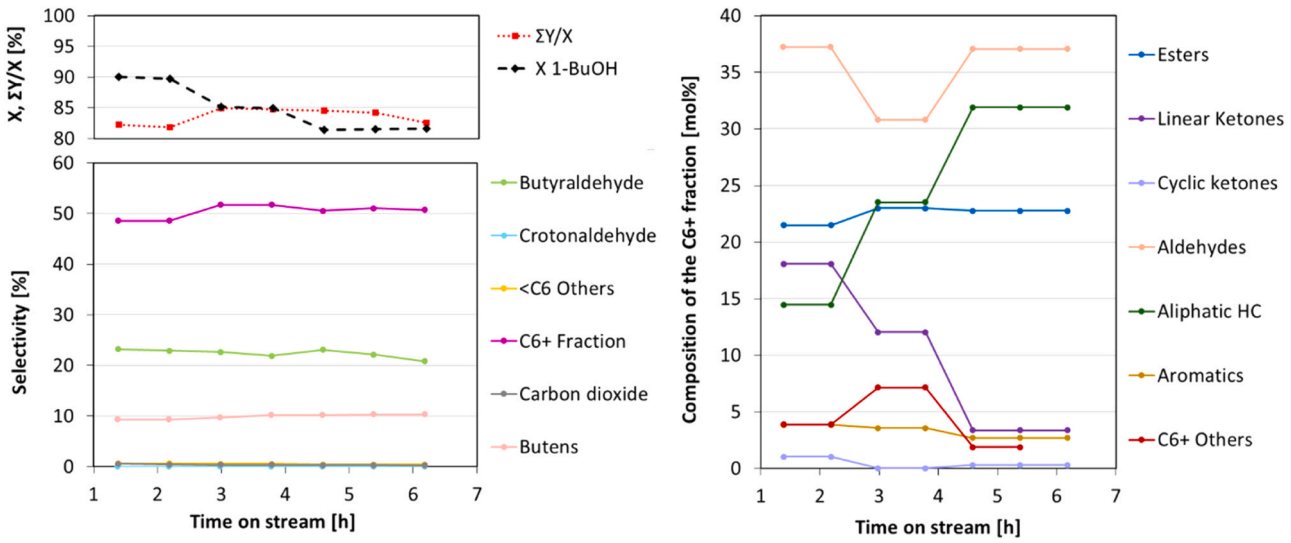

Fig. 12. Left, Conversion of BuOH (X BuOH), molar balance (ΣY/X) and products selectivity (S) as a function of time on stream over catalyst 5Cu/*t*-ZrO_2. Reaction conditions T = 300 °C, τ = 2 s, BuOH 10% in He. Right, Composition of the C6+ fraction expressed as molar fraction of each family of compounds normalized on the total of the C6+ fraction, as a function of time on stream.

mechanism and its promotion can shift the equilibrium towards higher molecular weights, thus increasing selectivity for the C6+ fraction, decreasing acetaldehyde selectivity and increasing stability. 1-Butanol, which can be obtained by fermentation of biomass just as ethanol, can also be used as a reactant in this one-pot approach with success. Several aspects of the reactivity of the catalytic system are still under investigation. In particular, the deactivation and high yields of acetaldehyde are critical drawbacks of the process and require further study to be overcome. The evaluation of longer reaction times, the regeneration of the most stable catalytic systems and the use of real matrixes of bioethanol will also need exploration, especially when considering the process from an industrial perspective. Finally, a systematic physicochemical analysis of the C6+ fraction will be paramount to guide the investigation towards the eventual match with the properties of commercial jet fuel blends.

CRediT authorship contribution statement

Fabrizio Cavani: Conceptualization, Funding acquisition, Supervision, Writing – review & editing. **Tommaso Tabanelli:** Conceptualization, Methodology, Supervision, Validation, Writing – review & editing. **Rita Mazzoni:** Supervision, Validation, Writing – review & editing. **Jacopo De Maron:** Data curation, Investigation, Methodology, Writing – review & editing. **Giulia Balestra:** Investigation, Methodology. **Anna Gagliardi:** Data curation, Investigation, Methodology, Writing – original draft.

Declaration of Competing Interest

The authors declare the following financial interests/personal relationships which may be considered as potential competing interests: Fabrizio Cavani reports financial support was provided by GST Gestioni Servizi Tecnologie S.r.l. Fabrizio Cavani reports financial support was provided by IG Operation and Maintenance S.p.A. If there are other authors, they declare that they have no known competing financial interests or personal relationships that could have appeared to influence the work reported in this paper.

Data availability

Data will be made available on request.

Acknowledgements

GST Gestioni Servizi Tecnologie S.r.l. and IG Operation and Maintenance S.p.A are acknowledged for the funding. TT and JDM also acknowledge funding from European Commission, NextGenerationEU – Piano Nazionale di Ripresa e Resilienza (PNRR) - Ministero dell'Università e della Ricerca (MUR); (project number PE_00000021).

Appendix A. Supporting information

Supplementary data associated with this article can be found in the online version at doi:10.1016/j.apcatb.2024.123865.

References

[1] K. Thanikasalam, M. Rahmat, A.G. Mohammad Fahmi, A.M. Zulkifli, N. Noor Shawal, K. Ilanchelvi, M. Ananth, R. Elayarasan, Ethanol content concerns in motor gasoline (mogas) in aviation in comparison to aviation gasoline (avgas), IOP Conf. Ser. Mater. Sci. Eng. 370 (2018) 012009, https://doi.org/10.1088/1757-899X/370/1/012009.
[2] A. Groysman, Corrosion in Systems for Storage and Transportation of Petroleum Products and Biofuels, Springer Netherlands, Dordrecht, 2014, https://doi.org/10.1007/978-94-007-7884-9.
[3] ReFuelEU Aviation initiative: Sustainable aviation fuels and the fit for 55 package | Think Tank | European Parliament, (n.d.). ⟨https://www.europarl.europa.eu/thinktank/en/document/EPRS_BRI(2022)698900⟩ (accessed August 9, 2022).
[4] E.B. Fox, Z.-W. Liu, Z.-T. Liu, Ultraclean fuels production and utilization for the twenty-first century: advances toward sustainable transportation fuels, Energy Fuels 27 (2013) 6335–6338, https://doi.org/10.1021/ef401094t.
[5] R. Mawhood, E. Gazis, R. Hoefnagels, S.D. Jong, Technological and commercial maturity of aviation biofuels: Emerging options to produce jet from lignocellulosic biomass, (2015) 10.
[6] F. Cheng, C.E. Brewer, Producing jet fuel from biomass lignin: Potential pathways to alkyl-benzenes and cycloalkanes, Renew. Sustain. Energy Rev. 72 (2017) 673–722, https://doi.org/10.1016/j.rser.2017.01.030.
[7] H. Wei, W. Liu, X. Chen, Q. Yang, J. Li, H. Chen, Renewable bio-jet fuel production for aviation: a review, Fuel 254 (2019) 115599, https://doi.org/10.1016/j.fuel.2019.06.007.
[8] G. Liu, B. Yan, G. Chen, Technical review on jet fuel production, Renew. Sustain. Energy Rev. 25 (2013) 59–70, https://doi.org/10.1016/j.rser.2013.03.025.
[9] N.A. Huq, G.R. Hafenstine, X. Huo, H. Nguyen, S.M. Tifft, D.R. Conklin, D. Stück, J. Stunkel, Z. Yang, J.S. Heyne, M.R. Wiatrowski, Y. Zhang, L. Tao, J. Zhu, C. S. McEnally, E.D. Christensen, C. Hays, K.M. Van Allsburg, K.A. Unocic, H. M. Meyer III, Z. Abdullah, D.R. Vardon, Toward net-zero sustainable aviation fuel with wet waste–derived volatile fatty acids, Proc. Natl. Acad. Sci. 118 (2021) e2023008118, https://doi.org/10.1073/pnas.2023008118.
[10] E.V. Fufachev, B.M. Weckhuysen, P.C.A. Bruijnincx, Toward catalytic ketonization of volatile fatty acids extracted from fermented wastewater by adsorption, ACS Sustain. Chem. Eng. 8 (2020) 11292–11298, https://doi.org/10.1021/acssuschemeng.0c03220.

[11] T. Roukas, P. Kotzekidou, Rotary biofilm reactor: a new tool for long-term bioethanol production from non-sterilized beet molasses by Saccharomyces cerevisiae in repeated-batch fermentation, J. Clean. Prod. 257 (2020) 120519, https://doi.org/10.1016/j.jclepro.2020.120519.

[12] S.M. Paixão, L. Alves, R. Pacheco, C.M. Silva, Evaluation of Jerusalem artichoke as a sustainable energy crop to bioethanol: energy and CO_2 eq emissions modeling for an industrial scenario, Energy 150 (2018) 468–481, https://doi.org/10.1016/j.energy.2018.02.145.

[13] A. Limayem, S.C. Ricke, Lignocellulosic biomass for bioethanol production: Current perspectives, potential issues and future prospects, Prog. Energy Combust. Sci. 38 (2012) 449–467, https://doi.org/10.1016/j.pecs.2012.03.002.

[14] T. Roukas, P. Kotzekidou, From food industry wastes to second generation bioethanol: a review, Rev. Environ. Sci. Biotechnol. 21 (2022) 299–329, https://doi.org/10.1007/s11157-021-09606-9.

[15] H. Chowdhury, B. Loganathan, Third-generation biofuels from microalgae: a review, Curr. Opin. Green. Sustain. Chem. 20 (2019) 39–44, https://doi.org/10.1016/j.cogsc.2019.09.003.

[16] R. Terán Hilares, S. Sanchez Muñoz, E.M. Alba, C.A. Prado, L. Ramos, M.A. Ahmed, S.S. da Silva, J.C. Santos, Recent technical advancements in first, second and third generation ethanol production. Prod. Top 12 Biochem. Sel. USDOE Renew. Resour., Elsevier, 2022, pp. 203–232, https://doi.org/10.1016/B978-0-12-823531-7.00009-3.

[17] Z. Li, A.W. Lepore, M.F. Salazar, G.S. Foo, B.H. Davison, Z. Wu, C.K. Narula, Selective conversion of bio-derived ethanol to renewable BTX over Ga-ZSM-5, Green. Chem. 19 (2017) 4344–4352, https://doi.org/10.1039/C7GC01188A.

[18] C.K. Narula, B.H. Davison, M. Keller, Zeolitic catalytic conversion of alcohols to hydrocarbons, US9533921B2, 2017.

[19] C.E. Wyman, J.R. Hannon, Systems and methods for improving yields of hydrocarbon fuels from alcohols, US11034891B2, 2021.

[20] C.E. Wyman, J.R. Hannon, Systems and methods for reducing energy consumption in production of ethanol fuel by conversion to hydrocarbon fuels, US10315965B2, 2019.

[21] C.E. Wyman, J.R. Hannon, Systems for reducing resource consumption in production of alcohol fuel by conversion to hydrocarbon fuels, US10815163B2, 2020.

[22] C.E. Wyman, J.R. Hannon, Systems and methods for reducing resource consumption in production of alcohol fuel by conversion to hydrocarbon fuels, WO2016201297A1, 2016.

[23] M.A. Lilga, R.T. Hallen, K.O. Albrecht, A.R. Cooper, J.G. Frye, K.K. Ramasamy, Systems and processes for conversion of ethylene feedstocks to hydrocarbon fuels, US 9663416 B2, 2017.

[24] V.L. Dagle, A.D. Winkelman, N.R. Jaegers, J. Saavedra-Lopez, J. Hu, M. H. Engelhard, S.E. Habas, S.A. Akhade, L. Kovarik, V.-A. Glezakou, R. Rousseau, Y. Wang, R.A. Dagle, Single-step conversion of ethanol to *n*-butene over Ag-ZrO_2/SiO_2 catalysts, ACS Catal. 10 (2020) 10602–10613, https://doi.org/10.1021/acscatal.0c02235.

[25] Z. Li, A. Lepore, B.H. Davison, C.K. Narula, Catalytic conversion of biomass-derived ethanol to liquid hydrocarbon blendstock: effect of light gas recirculation, Energy Fuels 30 (2016) 10611–10617, https://doi.org/10.1021/acs.energyfuels.6b02562.

[26] C.K. Narula, Z. Li, E.M. Casbeer, R.A. Geiger, M. Moses-Debusk, M. Keller, M. V. Buchanan, B.H. Davison, Heterobimetallic zeolite, InV-ZSM-5, enables efficient conversion of biomass derived ethanol to renewable hydrocarbons, Sci. Rep. 5 (2015) 16039, https://doi.org/10.1038/srep16039.

[27] A. Galadima, O. Muraza, Zeolite catalysts in upgrading of bioethanol to fuels range hydrocarbons: A review, J. Ind. Eng. Chem. 31 (2015) 1–14, https://doi.org/10.1016/j.jiec.2015.07.015.

[28] C.E. Wyman. Novel Vertimass Catalyst for Conversion of Ethanol and Other Alcohols into Fungible Gasoline, Jet, and Diesel Fuel Blend Stocks, 2015 http://www.energy.gov/sites/prod/files/2015/07/f24/wyman_bioenergy_2015.pdf.

[29] S. Geleynse, K. Brandt, M. Garcia-Perez, M. Wolcott, X. Zhang, The alcohol-to-jet conversion pathway for drop-in biofuels: techno-economic evaluation, ChemSusChem 11 (2018) 3728–3741, https://doi.org/10.1002/cssc.201801690.

[30] L. Harmon, R. Hallen, M. Lilga, B. Heijstra, I. Palou-Rivera, R. Handler, A Hybrid Catalytic Route to Fuels from Biomass Syngas, LanzaTech, Inc., 2017. ⟨https://www.osti.gov/servlets/purl/1423741⟩ (accessed October 29, 2022).

[31] Faster and Cheaper Ethanol-to-Jet-Fuel on the Horizon | PNNL, (n.d.). ⟨https://www.pnnl.gov/news-media/faster-and-cheaper-ethanol-jet-fuel-horizon⟩ (accessed October 29, 2022).

[32] Ethanol to Butenes in a Single Step | PNNL, (n.d.). ⟨https://www.pnnl.gov/available-technologies/ethanol-butenes-single-step⟩ (accessed October 29, 2022).

[33] Z. Habib, R. Parthasarathy, S. Gollahalli, Performance and emission characteristics of biofuel in a small-scale gas turbine engine, Appl. Energy 87 (2010) 1701–1709, https://doi.org/10.1016/j.apenergy.2009.10.024.

[34] K.K. Ramasamy, M.J. Gray, C.A. Alvarez-Vasco, M.F. Guo, S. Subramaniam, Conversion of Ethanol to C5+ ketones in single catalyst bed, US10221119B2, 2019.

[35] S. Subramaniam, M.F. Guo, T. Bathena, M. Gray, X. Zhang, A. Martinez, L. Kovarik, K.A. Goulas, K.K. Ramasamy, Direct catalytic conversion of ethanol to C_{5+} ketones: role of Pd–Zn alloy on catalytic activity and stability, Angew. Chem. Int. Ed. 59 (2020) 14550–14557, https://doi.org/10.1002/anie.202005256.

[36] K.K. Ramasamy, M.F. Guo, M.J. Gray, S. Subramaniam, Method of converting ethanol to higher alcohols, US10745330B2, 2020.

[37] K.K. Ramasamy, M.F. Guo, S. Subramaniam, U. Sanyal, C.O. Brady, Processes for the conversion of mixed oxygenates feedstocks to hydrocarbon fuels, US11492303B2, 2022.

[38] K. Kingsbury, P. Benavides, Life Cycle Inventories for Palladium on Niobium Phosphate (Pd/$NbOPO_4$) and Zirconium Oxide (ZrO_2) Catalysts, Technical report, U.S. Department of Energy, 2021. ⟨https://doi.org/10.2172/1784707⟩.

[39] K.A. Ali, A.Z. Abdullah, A.R. Mohamed, Recent development in catalytic technologies for methanol synthesis from renewable sources: a critical review, Renew. Sustain. Energy Rev. 44 (2015) 508–518, https://doi.org/10.1016/j.rser.2015.01.010.

[40] K. Li, J.G. Chen, CO_2 Hydrogenation to methanol over ZrO_2-containing catalysts: insights into ZrO_2 induced synergy, ACS Catal. 9 (2019) 7840–7861, https://doi.org/10.1021/acscatal.9b01943.

[41] Y. Zhu, J. Zheng, J. Ye, Y. Cui, K. Koh, L. Kovarik, D.M. Camaioni, J.L. Fulton, D. G. Truhlar, M. Neurock, C.J. Cramer, O.Y. Gutiérrez, J.A. Lercher, Copper-zirconia interfaces in UiO-66 enable selective catalytic hydrogenation of CO_2 to methanol, Nat. Commun. 11 (2020) 5849, https://doi.org/10.1038/s41467-020-19438-w.

[42] C. Mateos-Pedrero, C. Azenha, P.T. D.a, J.M. Sousa, A. Mendes, The influence of the support composition on the physicochemical and catalytic properties of Cu catalysts supported on Zirconia-Alumina for methanol steam reforming, Appl. Catal. B Environ. 277 (2020) 119243, https://doi.org/10.1016/j.apcatb.2020.119243.

[43] F. Bossola, N. Scotti, F. Somodi, M. Coduri, C. Evangelisti, V. Dal Santo, Electron-poor copper nanoparticles over amorphous zirconia-silica as all-in-one catalytic sites for the methanol steam reforming, Appl. Catal. B Environ. 258 (2019) 118016, https://doi.org/10.1016/j.apcatb.2019.118016.

[44] M. Śliwa, K. Samson, Steam reforming of ethanol over copper-zirconia based catalysts doped with Mn, Ni, Ga, Int. J. Hydrogen Energy 46 (2020) 555–564, https://doi.org/10.1016/j.ijhydene.2020.09.222.

[45] V. Shahed Gharahshiran, M. Yousefpour, V. Amini, A comparative study of zirconia and yttria promoted mesoporous carbon-nickel-cobalt catalysts in steam reforming of ethanol for hydrogen production, Mol. Catal. 484 (2020) 110767, https://doi.org/10.1016/j.mcat.2020.110767.

[46] T. Tsoncheva, I. Genova, M. Dimitrov, E. Sarcadi-Priboczki, A.M. Venezia, D. Kovacheva, N. Scotti, V. dal Santo, Nanostructured copper-zirconia composites as catalysts for methanol decomposition, Appl. Catal. B Environ. 165 (2015) 599–610, https://doi.org/10.1016/j.apcatb.2014.10.058.

[47] P. Liu, Y. Yang, M.G. White, Theoretical perspective of alcohol decomposition and synthesis from CO2 hydrogenation, Surf. Sci. Rep. 68 (2013) 233–272, https://doi.org/10.1016/j.surfrep.2013.01.001.

[48] A. Białas, T. Kondratowicz, M. Drozdek, P. Kuśtrowski, Catalytic combustion of toluene over copper oxide deposited on two types of yttria-stabilized zirconia, Catal. Today 257 (2015) 144–149, https://doi.org/10.1016/j.cattod.2015.01.005.

[49] N. Scotti, F. Zaccheria, C. Evangelisti, R. Psaro, N. Ravasio, Dehydrogenative coupling promoted by copper catalysts: a way to optimise and upgrade bio-alcohols, Catal. Sci. Technol. 7 (2017) 1386–1393, https://doi.org/10.1039/C6CY02670B.

[50] N. Scotti, N. Ravasio, F. Zaccheria, A. Irimescu, S.S. Merola, Green pathway to a new fuel extender: continuous flow catalytic synthesis of butanol/butyl butyrate mixtures, RSC Adv. 10 (2020) 3130–3136, https://doi.org/10.1039/D0RA00198H.

[51] N. Mansir, H. Mohd Sidek, S.H. Teo, N.-A. Mijan, A. Ghassan Alsultan, C.H. Ng, M. R. Shamsuddin, Y.H. Taufiq-Yap, Catalytically active metal oxides studies for the conversion technology of carboxylic acids and bioresource based fatty acids to ketones: a review, Bioresour. Technol. Rep. 17 (2022) 100988, https://doi.org/10.1016/j.biteb.2022.100988.

[52] J.W. Allen, A.M. Scheer, C.W. Gao, S.S. Merchant, S.S. Vasu, O. Welz, J.D. Savee, D. L. Osborn, C. Lee, S. Vranckx, Z. Wang, F. Qi, R.X. Fernandes, W.H. Green, M. Z. Hadi, C.A. Taatjes, A coordinated investigation of the combustion chemistry of diisopropyl ketone, a prototype for biofuels produced by endophytic fungi, Combust. Flame 161 (2014) 711–724, https://doi.org/10.1016/j.combustflame.2013.10.019.

[53] B. Almansour, G. Kim, S. Vasu, The effect of diluent gases on high-pressure laminar burning velocity measurements of an advanced biofuel ketone, SAE Int. J. Fuels Lubr. 11 (2018) 273–286, https://doi.org/10.4271/2018-01-0921.

[54] J. De Maron, L. Bellotti, A. Baldelli, A. Fasolini, N. Schiaroli, C. Lucarelli, F. Cavani, T. Tabanelli, Evaluation of the catalytic activity of metal phosphates and related oxides in the ketonization of propionic acid, Sustain. Chem. 3 (2022) 58–75, https://doi.org/10.3390/suschem3010005.

[55] T. Tabanelli, Unrevealing the hidden link between sustainable alkylation and hydrogen transfer processes with alcohols, Curr. Opin. Green. Sustain. Chem. 29 (2021) 100449, https://doi.org/10.1016/j.cogsc.2021.100449.

[56] T. Tabanelli, E. Paone, P. Blair Vásquez, R. Pietropaolo, F. Cavani, F. Mauriello, Transfer hydrogenation of methyl and ethyl levulinate promoted by a ZrO_2 catalyst: comparison of batch vs continuous gas-flow conditions, ACS Sustain. Chem. Eng. 7 (2019) 9937–9947, https://doi.org/10.1021/acssuschemeng.9b00778.

[57] P.B. Vásquez, T. Tabanelli, E. Monti, S. Albonetti, D. Bonincontro, N. Dimitratos, F. Cavani, Gas-phase catalytic transfer hydrogenation of methyl levulinate with ethanol over ZrO_2, ACS Sustain. Chem. Eng. 7 (2019) 8317–8330, https://doi.org/10.1021/acssuschemeng.8b06744.

[58] J. De Maron, M. Eberle, F. Cavani, F. Basile, N. Dimitratos, P. Maireles-Torres, E. Rodriguez Castellon, T. Tabanelli, Continuous-flow methyl methacrylate synthesis over gallium-based bifunctional catalysts, ACS Sustain. Chem. Eng. 9 (2021) 1790–1803, https://doi.org/10.1021/acssuschemeng.0c07932.

[59] W. Li, H. Huang, H. Li, W. Zhang, H. Liu, Facile synthesis of pure monoclinic and tetragonal zirconia nanoparticles and their phase effects on the behavior of supported molybdena catalysts for methanol-selective oxidation, Langmuir 24 (2008) 8358–8366, https://doi.org/10.1021/la800370r.

[60] K. Pokrovski, K.T. Jung, A.T. Bell, Investigation of CO and CO_2 adsorption on tetragonal and monoclinic zirconia, Langmuir 17 (2001) 4297–4303, https://doi.org/10.1021/la001723z.
[61] M. Ghiasi, A. Malekzadeh, Synthesis, characterization and photocatalytic properties of lanthanum oxy-carbonate, lanthanum oxide and lanthanum hydroxide nanoparticles, Superlattices Microstruct. 77 (2015) 295–304, https://doi.org/10.1016/j.spmi.2014.09.027.
[62] K.V.R. Chary, K.K. Seela, D. Naresh, P. Ramakanth, Characterization and reductive amination of cyclohexanol and cyclohexanone over Cu/ZrO_2 catalysts, Catal. Commun. 9 (2008) 75–81, https://doi.org/10.1016/j.catcom.2007.05.016.
[63] J.-Y. Park, Y.-J. Lee, P.K. Khanna, K.-W. Jun, J.W. Bae, Y.H. Kim, Alumina-supported iron oxide nanoparticles as Fischer–Tropsch catalysts: effect of particle size of iron oxide, J. Mol. Catal. Chem. 323 (2010) 84–90, https://doi.org/10.1016/j.molcata.2010.03.025.
[64] D.A.J.M. Ligthart, R.A. van Santen, E.J.M. Hensen, Influence of particle size on the activity and stability in steam methane reforming of supported Rh nanoparticles, J. Catal. 280 (2011) 206–220, https://doi.org/10.1016/j.jcat.2011.03.015.
[65] G. Balestra, J. De Maron, T. Tabanelli, F. Cavani, J. Lopez Nieto, The selective ethanol Guerbet condensation over alkali metal-doped sepiolite, Catal. Today (2023), https://doi.org/10.1016/j.cattod.2023.01.020.
[66] E.V. Makshina, W. Janssens, B.F. Sels, P.A. Jacobs, Catalytic study of the conversion of ethanol into 1,3-butadiene, Catal. Today 198 (2012) 338–344, https://doi.org/10.1016/j.cattod.2012.05.031.
[67] N. Miyake, G. Brezicki, R.J. Davis, Cascade reaction of ethanol to butadiene over multifunctional silica-supported Ag and ZrO_2 catalysts, ACS Sustain. Chem. Eng. 10 (2022) 1020–1035, https://doi.org/10.1021/acssuschemeng.1c07459.
[68] F. Zaccheria, N. Scotti, N. Ravasio, The role of copper in the upgrading of bioalcohols, ChemCatChem 10 (2018) 1526–1535, https://doi.org/10.1002/cctc.201701844.
[69] H. Idriss, E.G. Seebauer, Reactions of ethanol over metal oxides, J. Mol. Catal. Chem. 152 (2000) 201–212, https://doi.org/10.1016/S1381-1169(99)00297-6.
[70] A.-W. J. Al-Hamdany, Synthesis of substituted cyclohexenones from the condensation of acetone with 1,3-diaryl-2-propen-1-one, J. Educ. Sci. 23 (2010) 27–35, https://doi.org/10.33899/edusj.2010.59242.
[71] G.S. Salvapati, K.V. Ramanamurty, M. Janardanarao, Selective catalytic self-condensation of acetone, J. Mol. Catal. 54 (1989) 9–30, https://doi.org/10.1016/0304-5102(89)80134-8.
[72] R. Zheng, D. Liu, J. Tang, Q. Song, Q. Yao, Analysis of montmorillonite affecting coke formation during the thermal conversion of heavy oil, Fuel 288 (2021) 119687–119699.
[73] Ł. Smędowski, M. Krzesińska, W. Kwaśny, M. Kozanecki, Development of ordered structures in the high-temperature (HT) cokes from binary and ternary coal blends studied by means of x-ray diffraction and Raman spectroscopy, Energy Fuels 25 (2011) 3142–3149, https://doi.org/10.1021/ef200609t.
[74] E.V. Sagadeev, V.P. Barabanov, Calculations of the enthalpies of combustion of organic compounds by the additive scheme, Russ. J. Phys. Chem. 80 (2006) S152–S162, https://doi.org/10.1134/S0036024406130255.
[75] Y. Liu, Y. Yuan, G. Ramya, S. Mohan Singh, N. Thuy Lan Chi, A. Pugazhendhi, C. Xia, T. Mathimani, A review on the promising fuel of the future – Biobutanol; the hindrances and future perspectives, Fuel 327 (2022) 125166, https://doi.org/10.1016/j.fuel.2022.125166.